

**RESEARCH ARTICLE**

# Dendritic spine geometry and spine apparatus organization govern the spatiotemporal dynamics of calcium

Miriam Bell<sup>1</sup>, Tom Bartol<sup>2</sup>, Terrence Sejnowski<sup>2,3</sup>, and Padmini Rangamani<sup>1</sup> 

Dendritic spines are small subcompartments that protrude from the dendrites of neurons and are important for signaling activity and synaptic communication. These subcompartments have been characterized to have different shapes. While it is known that these shapes are associated with spine function, the specific nature of these shape–function relationships is not well understood. In this work, we systematically investigated the relationship between the shape and size of both the spine head and spine apparatus, a specialized endoplasmic reticulum compartment within the spine head, in modulating rapid calcium dynamics using mathematical modeling. We developed a spatial multicompartment reaction–diffusion model of calcium dynamics in three dimensions with various flux sources, including N-methyl-D-aspartate receptors (NMDARs), voltage-sensitive calcium channels (VSCCs), and different ion pumps on the plasma membrane. Using this model, we make several important predictions. First, the volume to surface area ratio of the spine regulates calcium dynamics. Second, membrane fluxes impact calcium dynamics temporally and spatially in a nonlinear fashion. Finally, the spine apparatus can act as a physical buffer for calcium by acting as a sink and rescaling the calcium concentration. These predictions set the stage for future experimental investigations of calcium dynamics in dendritic spines.

## Introduction

Dendritic spines, small protein- and actin-rich protrusions located on dendrites of neurons, have emerged as a critical hub for learning, memory, and synaptic plasticity in both short-term and long-term synaptic events (Bourne and Harris, 2008; Rangamani et al., 2016). These subcompartments provide valuable surface area for cell–cell interaction at synapses, and compartmentalization of signaling proteins to control and process incoming signals from the presynaptic terminal (Nishiyama and Yasuda, 2015; Yasuda, 2017). Thus, dendritic spines are hotbeds of electrical and chemical activity. Since calcium is the first incoming signal into the postsynaptic terminal, calcium temporal dynamics have been extensively studied experimentally and more recently computationally (Denk et al., 1996; Augustine et al., 2003; Bloodgood and Sabatini, 2005; Bartol et al., 2015b; Yasuda, 2017). In particular, calcium acts as a vital second messenger, triggering various signaling cascades that can lead to long-term potentiation, long-term depression, actin cytoskeleton rearrangements, and volume expansion, among other events (Holmes, 1990; Bourne and Harris, 2008; Rangamani et al., 2016).

Dendritic spine activity has numerous timescales, with signaling pathways operating on the millisecond to the hour timescale following spine activation (Yuste et al., 2000; Segal, 2005; Rangamani et al., 2016). Calcium dynamics are on the millisecond timescale, since calcium is the second messenger that floods the spine following the release of neurotransmitter from the presynaptic terminal. The temporal dynamics of calcium have provided valuable insight into the signaling dynamics in dendritic spines, and it is quite clear that calcium dynamics are influenced by a large number of factors. Multiple studies have connected the electrical activity of the plasma membrane (PM) voltage to calcium dynamics of N-methyl-D-aspartate receptors (NMDARs; Jahr and Stevens, 1993; Shouval et al., 2002; Rackham et al., 2010). The electrophysiology of dendritic spines influences many signaling dynamics through voltage-sensitive (or voltage-dependent) ion channels (Jaffe et al., 1994), and thus, models of these dynamics can be linked to downstream signaling.

Calcium is critical for almost all the reactions in the brain (Augustine et al., 2003) and is believed to accomplish a vast

<sup>1</sup>Department of Mechanical and Aerospace Engineering, University of California, San Diego, La Jolla, CA; <sup>2</sup>Howard Hughes Medical Institute, Salk Institute for Biological Studies, La Jolla, CA; <sup>3</sup>Division of Biological Sciences, University of California, San Diego, San Diego, CA.

Correspondence to Padmini Rangamani: [padmini.rangamani@engr.ucsd.edu](mailto:padmini.rangamani@engr.ucsd.edu).

© 2019 Bell et al. This article is distributed under the terms of an Attribution–Noncommercial–Share Alike–No Mirror Sites license for the first six months after the publication date (see <http://www.rupress.org/terms/>). After six months it is available under a Creative Commons License (Attribution–Noncommercial–Share Alike 4.0 International license, as described at <https://creativecommons.org/licenses/by-nc-sa/4.0/>).

variety of functions through localization (Clapham, 1995, 2007; Yuste and Denk, 1995). One possible way to achieve localization is by restricting the distance between the calcium source (often a channel) and the sink (calcium sensors and buffers). Thus, the localization of calcium can result from the location and mobility of different buffers and sensors (Schmidt, 2012). Spatial models of calcium dynamics in dendritic spines that consider such effects have been proposed previously (Holcman et al., 2004; Means et al., 2006; Bartol et al., 2015b). Spatial-temporal models of calcium dynamics have highlighted the role of calcium-induced cytosolic flow and calcium influx regulation by  $\text{Ca}^{2+}$ -activated  $\text{K}^+$  channels (SK channels; Holcman et al., 2004; Rackham et al., 2010). Computational studies using stochastic models of calcium transients have revealed that the readout of fluorescent probes can alter experimental readouts (Yuste et al., 2000; Higley and Sabatini, 2012; Bartol et al., 2015b). In particular, fluorescent probes can sequester calcium, effectively acting as calcium buffers and lowering the perceived calcium concentrations. Therefore, computational studies have already provided some insight into the spatiotemporal dynamics of calcium in both dendritic spines (Yuste et al., 2000; Segal, 2005; Rangamani et al., 2016) and whole neurons (Loewenstein and Sompolinsky, 2003). In this study, we specifically focus on the effect of spine geometry on calcium signals in the postsynaptic spine.

Recent advances in imaging and reconstruction techniques have shed light into the complex surface area of a single spine and the ultrastructure of the spine apparatus (SpApp; Kuwajima et al., 2013; Bartol et al., 2015a,b; Wu et al., 2017). Experimental evidence shows that calcium signals remain predominantly localized to single spines (Holmes, 1990; Koch and Zador, 1993; Sabatini et al., 2002). Dendritic spines have a unique set of shapes and recently the size and shape distribution of spines has been linked to their physiological function (Hering and Sheng, 2001; Berry and Nedivi, 2017). Additionally, only  $\sim 14\%$  of spines have a specialized ER known as the SpApp (Basnayake et al., 2018 Preprint; Jedlicka et al., 2008), which serves as a calcium store (Wuytack et al., 2002; Jedlicka et al., 2008). Indeed, calcium dynamics in dendritic spines are quite complex.

Given the importance of calcium dynamics in dendritic spines and the complexity of spine ultrastructure (Spacek and Harris, 1997; Holbro et al., 2009; Wu et al., 2017), we sought to use a computational approach to probe the role of spine geometry in modulating the spatiotemporal dynamics of calcium. Specifically, we seek to address the following questions: (i) How does the size and shape of both the spine head and SpApp affect calcium dynamics? (ii) How does the distribution of channels along the synaptic membrane modulate calcium dynamics within the spine? (iii) How do calcium buffers and calcium diffusion rates affect the spatiotemporal dynamics of calcium? To answer these questions, we develop a spatial 3-D reaction-diffusion model with multiple compartments. We chose a computational approach because it is not yet possible to manipulate spine size, shape, or SpApp location with precise control experimentally. However, the insights obtained from computational approaches can lay the groundwork for generating experimentally testable predictions (Kotaleski and Blackwell, 2010).

## Materials and methods

### Model assumptions

To interrogate the spatiotemporal dynamics of calcium in dendritic spines, we developed a reaction-diffusion model that accounts for the fluxes through the different sources and sinks shown in Fig. 1. We briefly discuss the assumptions made in developing this model and outline the key equations below. See Table 1 for common notation.

### Time scale

We model a single dendritic spine of a rat hippocampal area CA1 pyramidal neuron as an isolated system, because we focus on the 10- to 100-ms timescale and the ability of the spine neck to act as a diffusion barrier for calcium (Yuste and Denk, 1995; Bloodgood and Sabatini, 2005; Byrne et al., 2011; Gallimore et al., 2016). As a result, we do not consider calcium dynamics due to the mitochondria. This assumption is valid in our model, because even though mitochondria are known to act as calcium stores, their dynamics are on a longer timescale (10–100 s; Wacquier et al., 2016) and mitochondria are located in the dendrite outside of the dendritic spine. Although, it is well known that the SpApp acts as a source for calcium,  $\text{Ca}^{2+}$  release from the SpApp occurs at longer timescales because of  $\text{IP}_3$  receptors, RYR, and CICR (Jedlicka et al., 2008). It should also be noted that not all neurons have RYR and  $\text{IP}_3\text{R}$  on the SpApp (Mattson et al., 2000). Therefore, for the purpose and timescale of this study, we do not focus on CICR and therefore do not include RYR or  $\text{IP}_3\text{R}$  dynamics in this study.

### Membrane voltage stimulus

We model membrane voltage as an algebraic equation based on the summation of an excitatory postsynaptic potential (EPSP) and a back-propagating action potential (BPAP) applied to the entire PM (Jahr and Stevens, 1993; Shouval et al., 2002; Griffith et al., 2016). The EPSP arrives 2 ms before the BPAP to stimulate the maximum possible membrane depolarization (Fig. 1 d; Hu et al., 2018). This stimulus triggers the influx of calcium into the spine head.

### Spine head

The average spine head volume is  $\sim 0.03 \mu\text{m}^3$  (Spacek and Harris, 1997; Bartol et al., 2015b), but a large variation has been observed physiologically. The commonly observed shapes of dendritic spines include filopodia-like, stubby, short, and mushroom-shaped spines (Bourne and Harris, 2008; Berry and Nedivi, 2017). In this work, we consider two idealized geometries: a spherical spine head to represent a younger spine and an ellipsoidal spine head to represent a more mature mushroom spine (Spacek and Harris, 1997). The postsynaptic density (PSD) is modeled as a section of the membrane at the top of the spine head (Fig. 1 c). In simulations where the spine size is varied, we assume that the PSD changes surface area approximately proportionally to the spine head volume (Arellano et al., 2007).

### SpApp

SpApps are found primarily in larger mushroom spines (Spacek and Harris, 1997), which hints at their role in potential

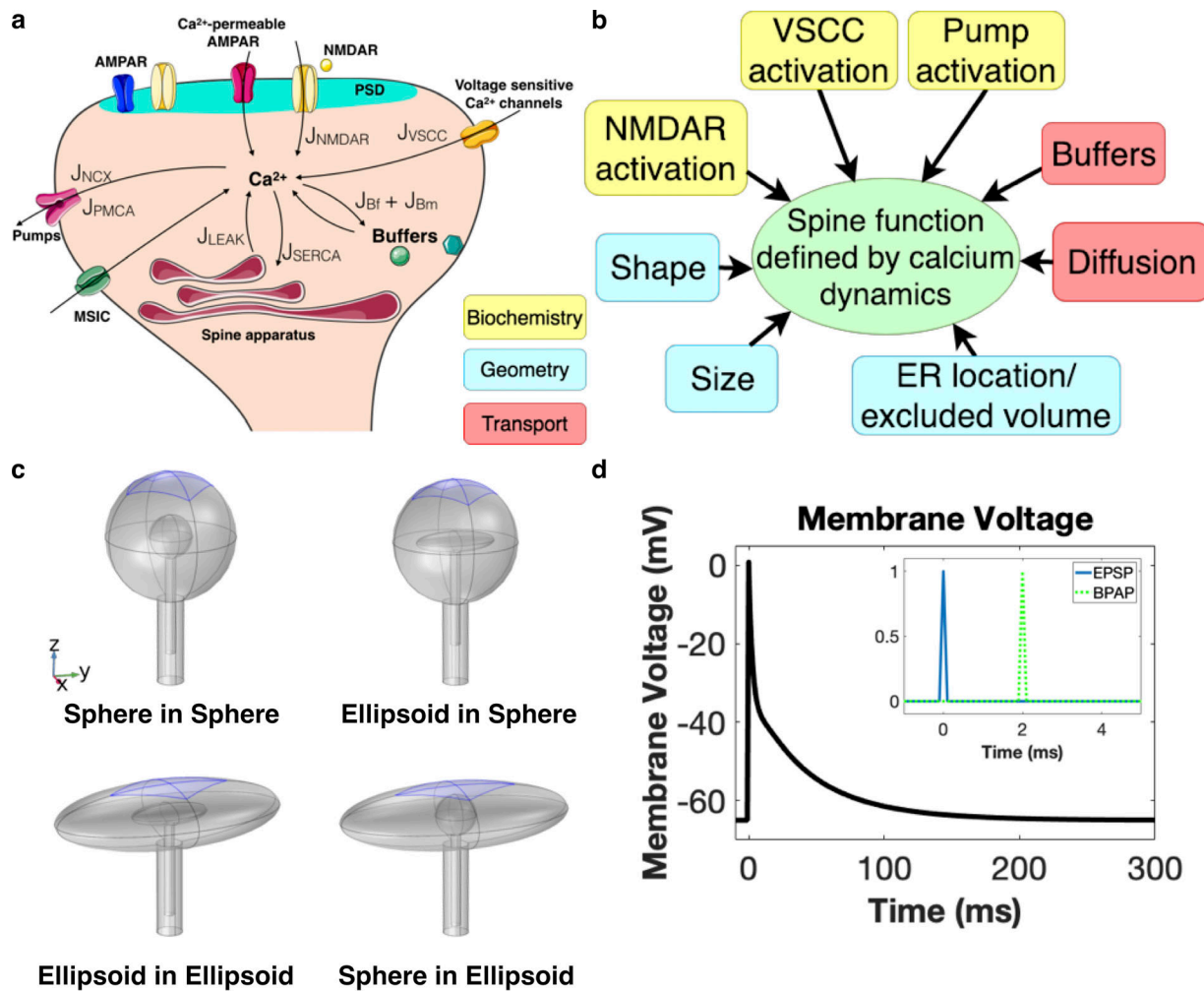


**Figure 1. Physical and chemical determinants of calcium influx in dendritic spines.** (a) Spatiotemporal dynamics of calcium in dendritic spines depend on multiple sources and sinks on both the spine membrane and the SpApp membrane. Fluxes are denoted as  $J_x$ , where  $x$  is the source or sink. These include receptors (NMDARs), channels (VSCCs), and pumps (PMCA and NCX). Calcium buffers are present both in the cytoplasm and on the PM.  $\alpha$ -amino-3-hydroxy-5-methyl-4-isoxazolepropionic acid receptor (AMPAR) is another important receptor that is often used as a readout for long term potentiation and depression. We do not include its dynamics in this model. (b) A partial list of factors that can influence these dynamics include biochemical components (shown in panel a), geometry, and protein transport components, which are effectively coupled through transport phenomena. In this study, we focus on the effects of spine and SpApp size, spine and SpApp shape, flux through NMDAR and VSCC distribution on calcium spatiotemporal dynamics, and buffers. (c) Four different combinations of spine head and SpApp geometries are used as model geometries (spherical head with spherical apparatus, spherical head with ellipsoidal apparatus, ellipsoidal head with ellipsoidal apparatus, and ellipsoidal head with spherical apparatus) to study how spine geometry affects calcium dynamics. The coordinate axes correspond to 100 nm in the different geometries. The blue shaded regions denote the PSD for each geometry. (d) In our model, depolarization of the membrane is triggered by an EPSP followed closely by a BPAP to create a maximal depolarization according to STDP. This membrane voltage acts as the input to our model. Inset: Timing of the EPSP and the BPAP. We model the maximum possible membrane depolarization based on STDP with the EPSP arriving 2 ms before the BPAP.

regulation of sustained spine volume (Ostroff et al., 2017). We assume that the SpApp acts as a calcium sink within the time-scale of interest (Segal et al., 2010). Another assumption is that the SpApp has the same shape as the spine head, a simplification of the more complicated and intricate SpApp geometry (Spacek and Harris, 1997).

#### PM fluxes

To maintain our focus on the short-timescale events associated with calcium dynamics, we include the following PM sources and sinks of calcium: voltage-sensitive calcium channels (VSCC), NMDARs, PM Ca<sup>2+</sup>-ATPase (PMCA) pumps, and sodium-calcium

exchanger (NCX) pumps. NMDARs are localized on the postsynaptic membrane adjacent to the PSD, designated at the top of the spine head. VSCC, PMCA, and NCX pumps are uniformly distributed along the PM, including at the base of the spine neck. Therefore, we model the dendritic spine as an isolated system with the spine neck base modeled in the same manner as the rest of the PM rather than explicitly modeling the base with an outward flux into the dendrite (see the following assumption).

#### Boundary condition at the base of the neck

We model the spine as an isolated system (Yuste and Denk, 1995; Sabatini et al., 2002; Bloodgood and Sabatini, 2005; Lee et al.,

Table 1. Notation used in this study

Variable/ parameter	Units	Definition/meaning
$Ca_{cyto}^{2+}$	$\mu M$	Calcium in the cytoplasm
$Ca_{ER}^{2+}$	$\mu M$	Calcium in the ER (SpApp)
D	$\frac{\mu m^2}{s}$	Diffusion rate
$B_m$	$\mu M$	Mobile buffers
$B_f$	Mol/ ( $\mu m^2$ s)	Fixed buffers
PDE		Partial differential equation
ODE		Ordinary differential equation
$J_x$	Mol/ ( $\mu m^2$ s)	Boundary flux due to x
CBP	$\mu M$	Calcium-binding proteins (calcium buffers)
$V_{cyto}$	$\mu m^3$	Volume of the cytoplasm excluding the SpApp volume
PM		Plasma membrane
SpApp		Spine apparatus
ECS		Extracellular space
n	$\mu m$	Scale factor to convert between volume reactions to boundary flux
$n_{PM}$	$\mu m$	Volume-to-surface area ratio of the cytoplasm to the PM
$n_{SpApp}$	$\mu m$	Volume-to-surface area ratio of the SpApp volume to the SpApp surface area
AUC	Ions/s	Area under the curve
EPSP	mV	Excitatory postsynaptic potential
BPAP	mV	Back-propagating action potential
NMDAR		N-methyl-D-aspartate receptor
VSCC		Voltage-sensitive calcium channel
PMCA		Plasma membrane calcium ATPase
NCX		Sodium-calcium exchanger

2009). Therefore, for most of our analyses, we use the same boundary conditions at the base of the spine neck as the rest of the PM. In the online supplemental material, we relax this assumption and test different boundary conditions, including a clamped calcium concentration at the base of the neck and an explicit effect of a dendritic shaft attached to the spine neck (Figs. S4 and S5).

#### Compartmental specific calcium ion concentration

We explicitly model calcium in the cytoplasm and in the SpApp. We assume that the calcium concentration in the extracellular space (ECS) is large enough (2 mM; Clapham, 1995; Bartol et al., 2015b) that the calcium influx into the spine has an insignificant effect on ECS calcium concentration. Therefore, ECS calcium concentration is assumed constant. We only solve the volumetric reactions in the cytoplasm. The ER calcium concentration is assumed to only affect the fluxes on the ER membrane.

#### Calcium-binding proteins (CBPs; buffers)

There are numerous CBPs present in the cytoplasm that act rapidly on any free calcium in the spine head (Yuste and Denk, 1995; Yuste et al., 2000; Sabatini et al., 2001, 2002; Bartol et al., 2015b). These CBPs are modeled as both mobile and fixed buffers in our system. Mobile buffers are modeled as volume components in the cytoplasm (Schmidt and Eilers, 2009; Schmidt, 2012), and they are modeled as a diffusive species with mass-action kinetics in the cytoplasm. We assume that the mobile buffers have a buffering capacity,  $\kappa$ , of 20, where  $\kappa = [B_m]/K_d$  (Sabatini et al., 2002; Matthews and Dietrich, 2015;  $B_m$  is the mobile buffer concentration;  $K_d$  is the dissociation constant). Dendritic spines also have fixed or immobile buffers, but the molecular identity of fixed buffers remains more elusive. Studies suggest that they are primarily membrane-bound components (Matthews and Dietrich, 2015); therefore, we model fixed buffers as immobile species localized to the PM. As a result, the interactions of calcium with these fixed buffers are treated as flux boundary conditions for the surface reactions with mass-action kinetics. We assume fixed buffers have a  $K_d = 2 \mu M$  (Bartol et al., 2015b) and have a concentration of  $78.7 \mu M$  (Bartol et al., 2015b). These values are converted to a membrane density by multiplying by the spine volume over PM surface area ( $n_{PM}$ ; see online supplemental material section S1.1 for more details.).

#### SpApp fluxes

In this model, the SpApp acts as a  $Ca^{2+}$  sink in the 10- to 100-ms timescale (Fifková et al., 1983; Fifková, 1985; Jedlicka et al., 2008). The implications of this assumption are discussed later in the paper. We assume that SERCA pumps are located uniformly on the SpApp membrane. SERCA pumps have been observed to buffer a large percentage of calcium within the spine, so we include SERCA pumps with a relatively large influx (Higley and Sabatini, 2012; Hu et al., 2018). We also include a small leak current from the SpApp to the cytoplasm and set this leak current to offset pump dynamics at basal calcium concentrations of 100 nM (Bartol et al., 2015b; Futagi and Kitano, 2015).

Based on these assumptions, we constructed a 3-D spatial model of  $Ca^{2+}$  dynamics in dendritic spines. Our control geometry is a medium-sized spine with volume of  $\sim 0.06 \mu m^3$  including the spine head and neck, with a SpApp of volume  $\sim 0.003 \mu m^3$ . We use a spherical spine with spherical SpApp and ellipsoidal spine with ellipsoidal SpApp as our two control spines of interest. Most results are shown as a 2-D cross section for ease of interpretation (see Fig. S7 for examples of the full 3-D solutions).

#### Spatial model of $Ca^{2+}$ influx

The spatiotemporal dynamics of calcium are determined by the combination of dynamics within the spine volume and boundary conditions at the PM and SpApp. Calcium dynamics in the spine volume are represented by a single reaction-diffusion equation:

$$\frac{\partial Ca^{2+}}{\partial t} = D \nabla^2 Ca^{2+} - f(Ca_{cyto}^{2+}, CBP). \quad (1)$$

Here, D is the diffusion coefficient of calcium and  $f(Ca_{cyto}^{2+}, CDP)$  is a function that represents the reaction between cytosolic

calcium and mobile buffers in the cytoplasm;  $\nabla^2$  is the Laplacian operator in three dimensions. The stimulus to the system is the depolarization of the membrane based on an EPSP and BPAP separated by 2 ms (Fig. 1 d). The boundary conditions at the PM and the SpApp are given by time-dependent fluxes that represent the kinetics of different channels, pumps, and fixed buffers.

### Boundary conditions at the PM

We model the calcium influx through activated NMDARs in response to glutamate release in the synaptic cleft and the calcium influx through VSCCs in response to membrane depolarization (Jahr and Stevens, 1993; Shouval et al., 2002; Bartol et al., 2015b). We should note that the majority of existing models for NMDAR and VSCC calcium influx assume well-mixed conditions. In this model, these species are restricted to the PM, which is the boundary of the geometry. This results in a time-dependent flux at the PM. Both the NMDAR and VSCC-mediated calcium influx depend on the membrane voltage (see Fig. 1 d); we prescribe this voltage as a set of biexponentials to capture a BPAP and EPSP based on previous studies (Jahr and Stevens, 1993; Shouval et al., 2002). On the PM, we also include PMCA and NCX that are activated in response to a change in cytosolic calcium concentration (Calizo et al., 2017 *Preprint*; Maurya and Subramaniam, 2007). We also localize fixed CBPs (fixed buffers) to the PM. Therefore, the binding of cytosolic calcium to fixed buffers ( $B_f$ ) is modeled as a membrane flux,  $J_{Bf}$ . The flux boundary condition at the PM is then the sum of all these fluxes and is given by

$$-D(n \cdot \nabla Ca^{2+})|_{PM} = J_{NMDAR} + J_{VSCC} - J_{PMCA} - J_{NCX} - J_{Bf}. \quad (2)$$

The functions that define the flux terms in Eq. 2 are given in Table S1.

### Boundary condition at the SpApp membrane

In the cases where we included a SpApp, we included SERCA pumps and a leak term along the SpApp membrane that are functions of the cytosolic calcium concentration. The boundary condition for the flux across the SpApp membrane is given by

$$-D(n \cdot \nabla Ca)|_{SpApp} = J_{SERCA} - J_{LEAK}. \quad (3)$$

The functions that define the flux term in Eq. 3 are given in Table S1.

To briefly summarize, these governing equations are simply the balance equations that keep track of the spatio-temporal dynamics of cytosolic calcium due to calcium diffusion and mobile buffers (Eq. 1), influx and efflux through the PM (Eq. 2), and influx and efflux through the SpApp membrane (Eq. 3). The coupled nature of this system of equations and time-dependent fluxes limits the possibility of obtaining analytical solutions even for simple geometries (Cugno et al., 2018 *Preprint*). Therefore, we use computational methods to solve these equations.

### Parametric sensitivity analyses

Given the vast number of parameters in this model, we constrain the parameters in our model as follows: parameter values are chosen from experimental observations or existing

computational models or to match overall experimental and computational observations with respect to pump or channel dynamics (section S1). Overall, we predict a high calcium concentration and relatively fast decay dynamics (Sabatini et al., 2002; Higley and Sabatini, 2012; Hu et al., 2018). See Fig. S2 for a comparison of temporal dynamics to existing literature. We conducted a kinetic parameter sensitivity analysis for our model using the open source software COPASI—a CComplex PAthway SImulator (Supplemental text). The sensitivity analysis was performed in COPASI by converting our spatial model into a compartmental ordinary differential equation (ODE) system. This conversion involves transforming boundary flux equations into volumetric reaction rate through the lengthscale factor  $n$ , the volume-to-surface area ratio.

### Geometries used in the model

We modeled the dendritic spines using idealized geometries of spheres and ellipsoids; dendritic spines consist of a spine head attached to a neck, with a similarly structured SpApp within the spine, see Fig. 1 c for the different model geometries used in this study. These geometries were inspired by reconstructions (Bartol et al., 2015a; Griffith et al., 2016; Paulin et al., 2016) and were idealized for ease of computation. For the variations of the base of the neck, we also include a condition with an explicit dendrite modeled as a cylinder attached to the spine neck, Figs. S4 and S5. The geometric parameters, including volume and surface area, are given in Table S8.

### Numerical methods

Simulations for calcium dynamics were conducted using commercial finite-element software (COMSOL Multiphysics 5.4). Specifically, the general form and boundary partial differential equations (PDEs) interface were used and time-dependent flux boundary conditions were prescribed. A user-defined tetrahedral mesh with a maximum and minimum element size of 0.0574  $\mu\text{m}$  and 0.00717  $\mu\text{m}$ , respectively, was used. Due to the time-dependent, nonlinear boundary conditions used in this model, we also prescribed four boundary layers (prism mesh elements) on all membranes in COMSOL. A time-dependent solver was used to solve the system, specifically a MUMPS (MULTifrontal Massively Parallel sparse direct Solver) solver with backward differentiation formula time-stepping method with a free time stepper. Results were exported to MATLAB for further analysis. All COMSOL files will be posted on the Rangamani Lab website for public dissemination.

### Online supplemental material

All model equations and parameters and geometric parameters can be found in the online supplemental material. Fig. S1 shows the effects due to using a different lengthscale,  $n$ . Fig. S2 shows temporal comparison with other existing models. Fig. S3 is a sensitivity analysis of model parameters. Figs. S4 and S5 show the case when the neck base has different boundary conditions in spherical and ellipsoidal spines, respectively. Fig. S6 shows the effect of spine neck radius. Fig. S7 shows calcium spatial dynamics in 3D for spherical and ellipsoidal spines. Fig. S8 shows temporal dynamics and peak concentrations for spines of

various shapes. Fig. S9 shows the effects of different calcium buffers in ellipsoidal spines. Table S1 lists the main equations in the model. Table S2 lists parameters used in the model for the volumes. Table S3 lists parameters for NMDAR. Table S4 lists parameters for membrane voltage. Table S5 lists parameters for VSCC. Table S6 lists parameters for PMCA and NCX pumps. Table S7 lists parameters for SERCA. Table S8 lists the size and shape parameters of the different geometries. Table S9 lists size variations for the spherical spine head with spherical SpApp. Table S10 lists size variations for the ellipsoidal spine head with ellipsoidal SpApp. Table S11 lists size variations for the spherical spine head with spherical SpApp when varying SpApp volume. Table S12 lists size variations for the ellipsoidal spine head with ellipsoidal SpApp when varying SpApp volume.

## Results

Using the model developed above (Eqs. 1–3), we investigated how different geometric factors of the spine head and SpApp affect calcium dynamics. Because of the coupling between the volume dynamics (Eq. 1) and the fluxes on the membranes due to biochemical components (Eqs. 2 and 3), the effect of spine geometry on calcium dynamics is quite complex. To parse the coupled effects, we have categorized and organized our simulations as follows and discuss each case in detail. First, we investigated the effect of spine volume to surface area ratio. This parameter can be changed in multiple ways: by changing the shape of the spine head and the shape or presence of the SpApp (Figs. 2 and 3), by changing the size of the spine head alone (Fig. 4), or by changing the size of the SpApp alone (Fig. 5). Next, we investigated the effect of spatial distribution of the fluxes on the PM (Fig. 6). Finally, we demonstrate the effect of buffer types and their location (Figs. 7 and 8). We describe each of these results in detail below.

### Effect of spine volume to surface area on calcium dynamics

#### Effects of shape of the spine head and the shape of the SpApp on calcium dynamics

We first analyzed how the volume to surface area ratio of the spine affects the spatiotemporal dynamics of calcium by simulating calcium dynamics in the different geometries shown in Fig. 1c. All of these geometries were constructed such that they have the same volume of the spine cytosol but the surface area of the PM and SpApp vary because of the shape (Table S8). We note that in all the geometries, the temporal dynamics of calcium shows a rapid increase in the first 2–3 ms and a decay over ~50 ms (Fig. S8). This time course is consistent with experimentally observed and computationally modeled calcium dynamics (Ngo-Anh et al., 2005; Matthews et al., 2013; Hu et al., 2018; Figs. 2d and S2, respectively). The spatial profiles of calcium in spheres and ellipsoids (Fig. 2, a and b) show that spine shape can alter the spatial gradients and decay profiles of calcium. In particular, we observe that while at 5 ms all shapes demonstrate a gradient from the PSD region to the spine neck, because of the localized influx of calcium through the NMDAR in the PSD, at 10 ms, the ellipsoidal spine heads have almost no gradient within the spine head. Instead, they have a more

pronounced difference between the spine head and spine neck. We also changed the shape of the SpApp to get different combinations of spine head and SpApp geometries (Fig. 2). Since the apparatus acts as a sink, we find that the reduction in surface area to volume ratio of the spherical apparatus leads to less influx into the SpApp, compared with the ellipsoidal SpApp (Fig. 2c). This result emphasizes the nonintuitive relationships between organelle shape and spine shape.

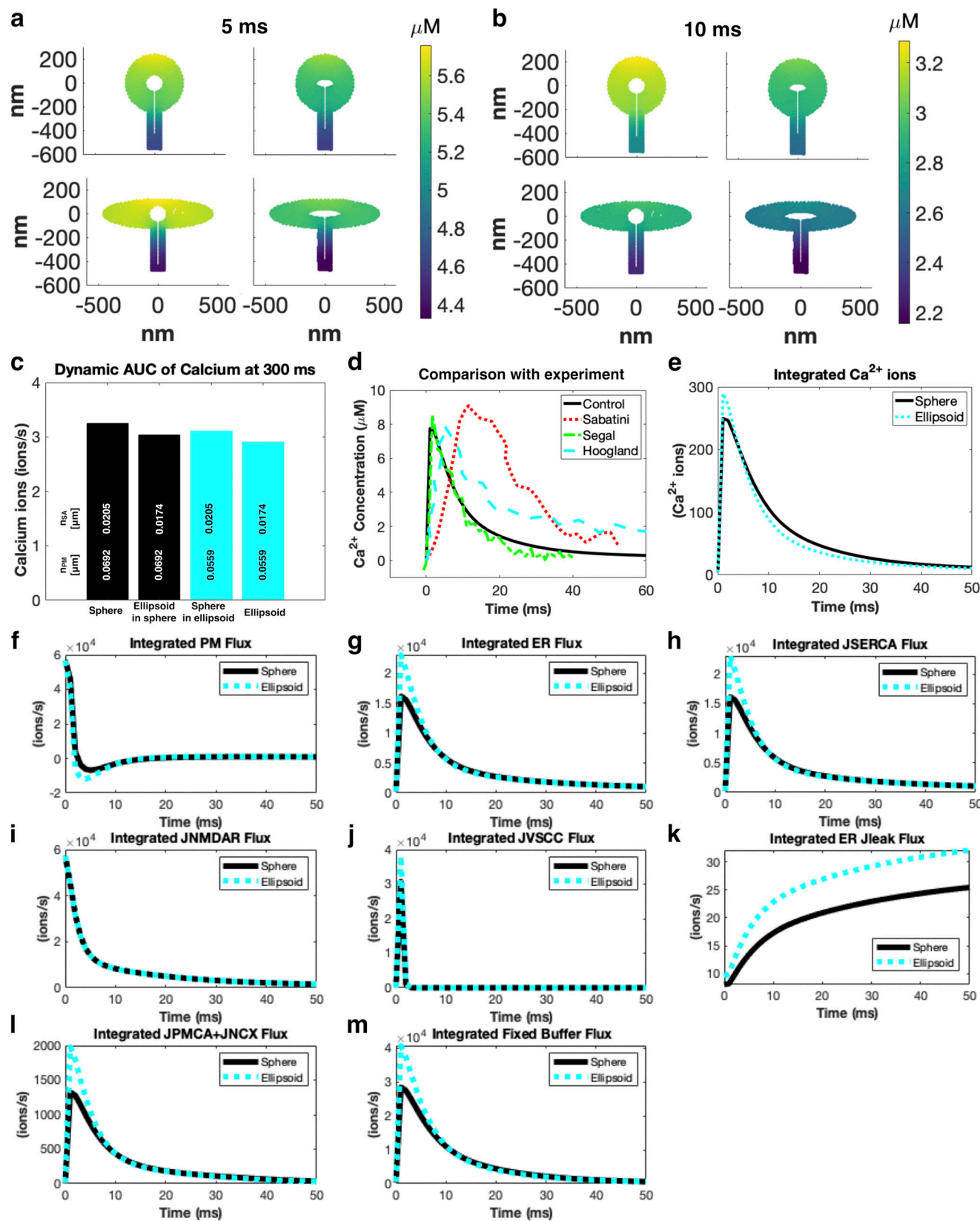
In addition to the transient response of calcium, the cumulative calcium (total calcium) also carries information with respect to synaptic plasticity (Bourne and Harris, 2008; Rangamani et al., 2016; Basak and Narayanan, 2018). Therefore, we calculated the integrated calcium over the entire spine volume (area under the curve [AUC]; Gorman and Sejnowski, 1988; Heinrich et al., 2002; Atay and Skotheim, 2017) over 300 ms. Calcium AUC at 300 ms (Fig. 2c) shows that all spines have slightly different accumulated calcium. Upon closer examination of the membrane fluxes of the sphere and ellipsoid spines (Fig. 2, e–m), we see that there is a complex relationship between the calcium ion concentration and nonlinear flux terms. In particular, the higher calcium influx in the ellipsoids due to the larger surface area leads to a higher efflux of calcium through the PMCA, NCX, and SERCA pumps and increased binding to fixed buffers on the PM. Therefore, the nonlinear effects of the fluxes associated with the pumps reduces the difference in calcium between spines of different shapes.

#### Effects of the presence/absence of the SpApp on volume to surface area

Another way to modulate the volume to surface area ratio is to consider spines with and without the SpApp. In our model, the SpApp serves both as a calcium sink through SERCA pumps and as an excluded volume. We observe that the presence of the SpApp in both spheres and ellipsoids (Fig. 3, a and d, top row) results in a steeper gradient from the PSD to the neck when compared with the spines without a SpApp (Fig. 3, a and d, bottom row). Additionally, at 10 ms, spines without a SpApp have a higher calcium concentration than spines with a SpApp. This is because the dynamics of calcium are altered in the presence of the SpApp by the SERCA fluxes, Eq. 3. As a result, regardless of the shape, spines with a SpApp have a faster decay of cytosolic calcium (Fig. 3, b and e). We found that in both geometries, the AUC of spines with a SpApp was lower at different time points when compared with spines without a SpApp (Fig. 3, c and f). At 300 ms, the spine without a SpApp has 47.75% more total calcium for the spherical geometry and 49.09% more for the ellipsoidal geometry. Thus the flux due to SERCA plays a significant role in altering the decay dynamics of calcium in spines with SpApp and as a result alters the total calcium.

#### Effect of spine volume on calcium dynamics

In addition to spine shape, spine size (volume) is also known to change during development and plasticity related events (Knott et al., 2006; Kasai et al., 2010; Rangamani et al., 2016). How does changing the volume of the spine, while maintaining the same shape, affect calcium dynamics? To answer this question, we conducted simulations in spherical and ellipsoidal spines of



Downloaded from https://jgp.rupress.org/particles/pdf/151/8/1017/180492/jgp-20181226-1.pdf by guest on 08 February 2026

**Figure 2. Spine head volume-to-surface area ratio modifies calcium dynamics through membrane flux contributions.** (a and b) Spatial distribution of calcium in spines at two different time points (5 ms [a] and 10 ms [b]). The instantaneous gradient of calcium ions depends on the shape of the spine head and the shape of the SpApp. (c) Calcium accumulation at 300 ms was calculated using the AUC of the spatial and temporal dynamics of calcium throughout the volume; the differences between the shapes are small, with the most pronounced difference being a 12% increase in AUC between the sphere and ellipsoid

spines. (d) We plot the temporal dynamics at the top of the spherical control spine versus reported experimental calcium transients from previous studies (Sabatini et al., 2002; Hoogland and Saggau, 2004; Segal and Korkotian, 2014). The experimental transients are reported in terms of fluorescence, which we assume are linearly proportional to concentration (Yasuda et al., 2004). We plot Fig. 1 F from Sabatini et al. (2002), Fig. 1 from Segal and Korkotian (2014), and Fig. 2 D from Hoogland and Saggau (2004). PlotDigitizer was used to trace the temporal profiles that were then plotted in MATLAB. We more closely compared the spherical and ellipsoidal spines by integrating total calcium ions over time (e) and considering the integrated fluxes for both shapes (f-m). We see that the ellipsoid has more calcium ions than the sphere (e), because despite having more calcium influx due to VSCC (j), the subsequent higher calcium concentration leads to higher efflux due to pumps (h and l) and buffers (m). Note the timescale in panels e-m is shortened to 50 ms for clarity.

different volumes. Recall that the control spine has a cytosolic volume,  $V_{cyto}$ , of  $0.06 \mu\text{m}^3$  (Table S8). For each geometry (sphere and ellipsoid), we maintained the same size and shape of the

SpApp as before and only changed the spine cytoplasm volume in the range of  $0.5 V_{cyto}$  to  $1.5 V_{cyto}$  (Tables S9 and S10). We found that the relationship between spine volume and calcium

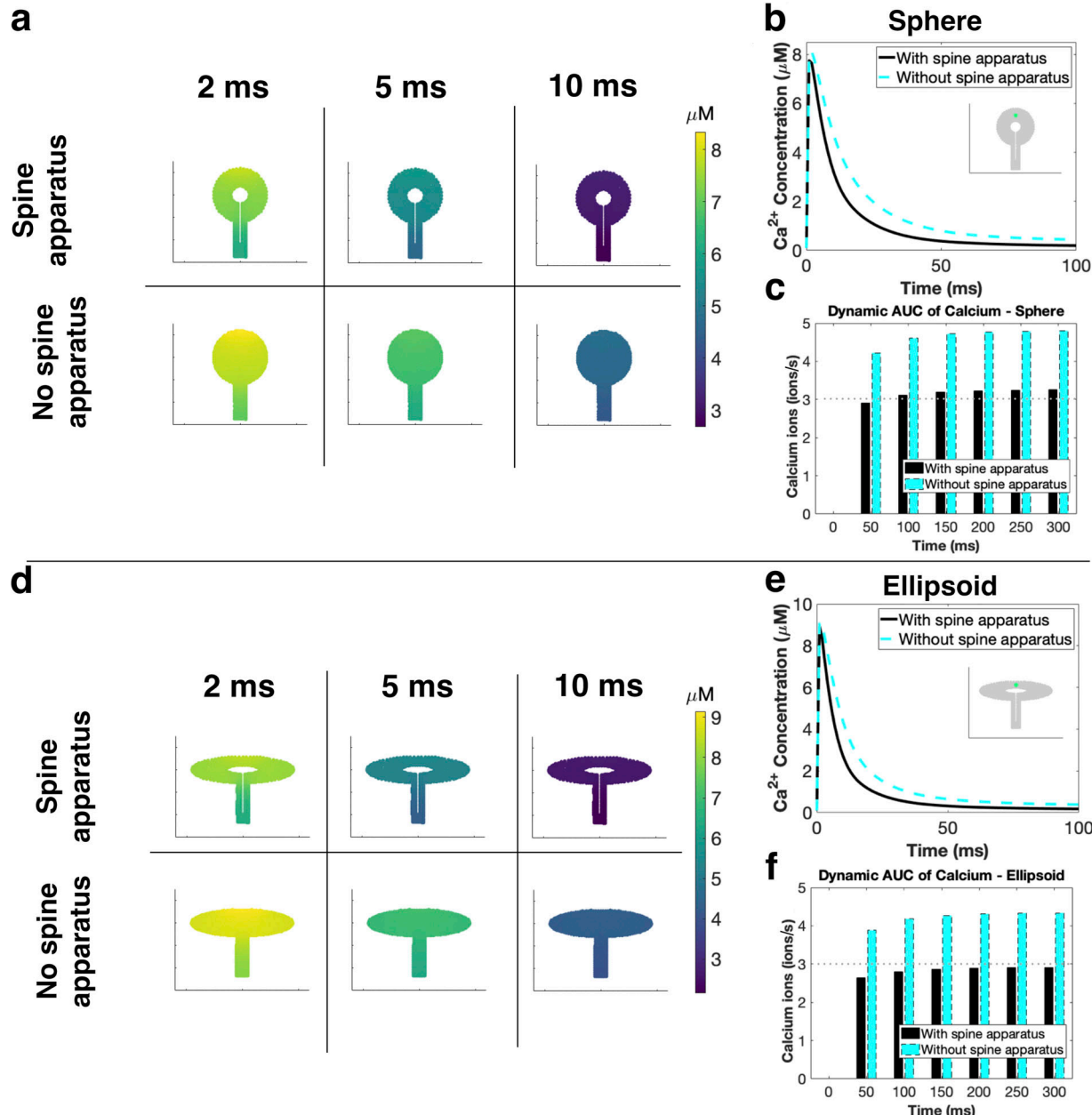


**Figure 3. The presence of a SpApp, acting as a sink, modulates calcium dynamics.** Spines without SpApp have higher and more sustained calcium activity despite their increased volume in both spherical (a) and ellipsoidal (d) spines. Temporal dynamics (b and e) and AUC (c and f) plots show that the absence of a SpApp (no SERCA flux, denoted as  $J_{SERCA}$ ) leads to a prolonged calcium transient and higher total calcium levels for both spherical and ellipsoidal shapes. Insets in panels b and e show the location in the spine from where the time courses were plotted.

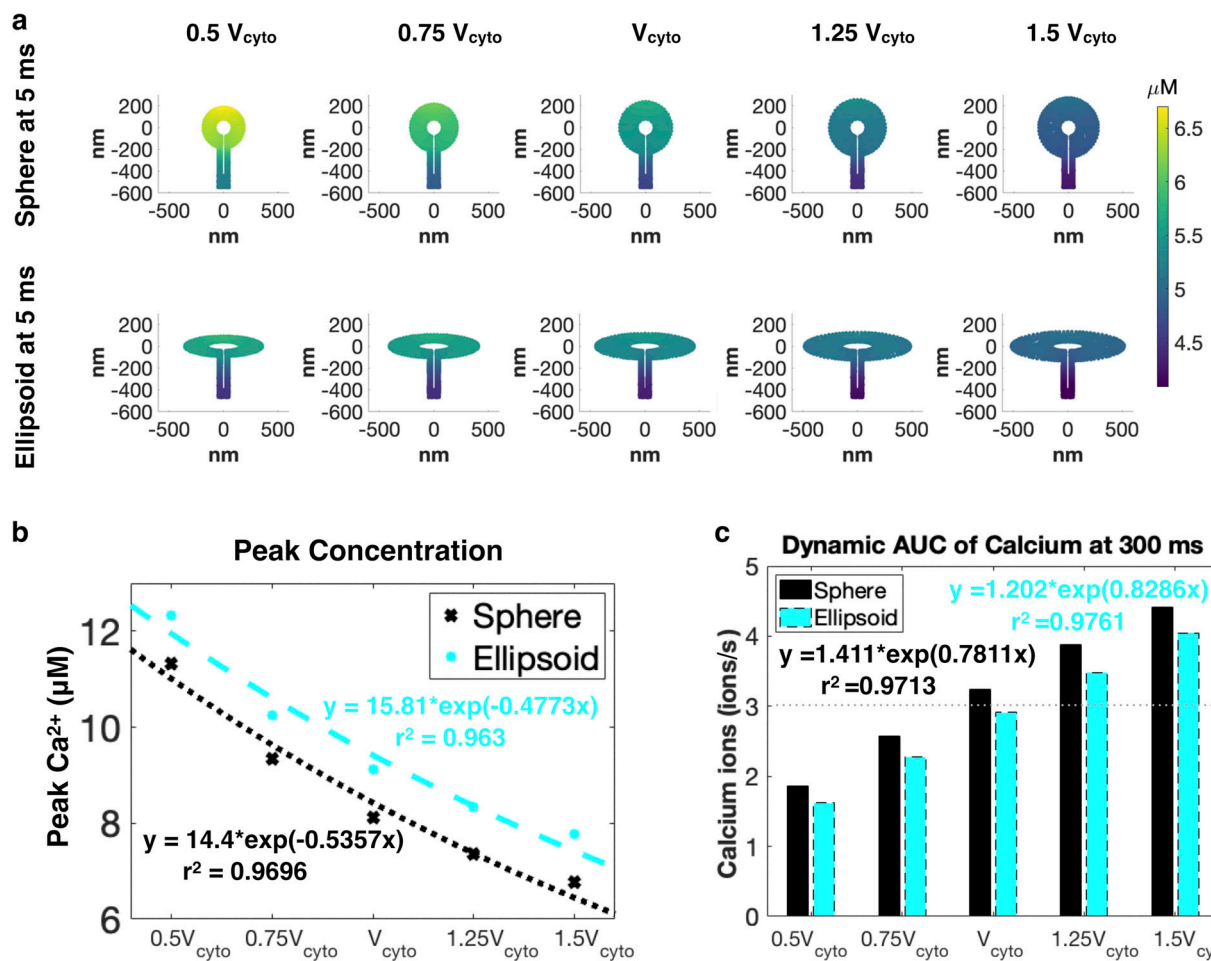


**Figure 4. Accumulated calcium scales inversely proportional to the spine head volume.** (a) Calcium dynamics in spines of different sizes show that as spine volume increases, calcium concentration in the spine decreases. The effect of spine size on the temporal dynamics of calcium is seen in the peak values (b) and AUCs of calcium (c). Increasing spine volume decreases the peak calcium concentration but increases overall AUC in the spine irrespective of the spine shape. cyto, cytoplasm.

concentration is inversely proportional. For spine volumes smaller than the control, we observed an increase in calcium concentration for both geometries, whereas for larger volumes, calcium concentration decreases (Fig. 4, a and b). As expected, we found that for both geometries, an increase in spine volume resulted in an increase in cumulative calcium (Fig. 4 c). Furthermore, we found that the change in cumulative calcium has a direct but nonlinear relationship with the change in spine volume. For the range of volumes investigated, the peak calcium concentration and AUC show an exponential relationship with respect to volume. We see at all sizes the ellipsoid has higher peak concentrations but lower AUC compared with the sphere.

#### Effect of SpApp size and geometry

The complex architecture of the SpApp was recently elucidated in a focused ion beam scanning electron microscopy study by Wu et al. (2017). Since we cannot yet manipulate the shape of the SpApp *in vivo*, we varied the geometric features of the SpApp *in silico* to see how they affect calcium dynamics. Previously, we showed that SpApp shape and spine volume separately can alter the AUC and peak calcium. Here, for a given spine shape, we

varied the volume of the SpApp to modulate the cytosolic volume to SpApp volume ratio. In this case, by varying the SpApp volume, we altered the spine volume to be 50% and 75% of V<sub>cyto</sub>, the control spine volume. Here, we change the spine volume by the changing SpApp size (Fig. 5). We found that a larger SpApp leads to a decrease in calcium concentrations and AUC (Fig. 5, a and c) but an increase in peak concentration (Fig. 5 b). We note that as SpApp volume increases, AUC drops in a nonlinear manner in both geometries. The spherical spine has a 55.4% and 77.8% reduction in AUC from control for the 75% and 50% spines, while the ellipsoidal spine has a 57.2% and 79.4% reduction from control. For all sizes, the ellipsoid shows higher peak concentrations but lower AUC compared with the sphere. This effect is in part due to the shortened distance between the PSD and SpApp in the ellipsoid. The distance between the PSD and SpApp is an important lengthscale in the spine, since it controls the distance between the sources and sinks of calcium. Therefore, changing this lengthscale, as happens when changing the SpApp volume, influences calcium dynamics in nonlinear ways. From these observations, we conclude that spine volume coupled with SpApp volume and surface area is an important regulator of calcium dynamics in dendritic spines.

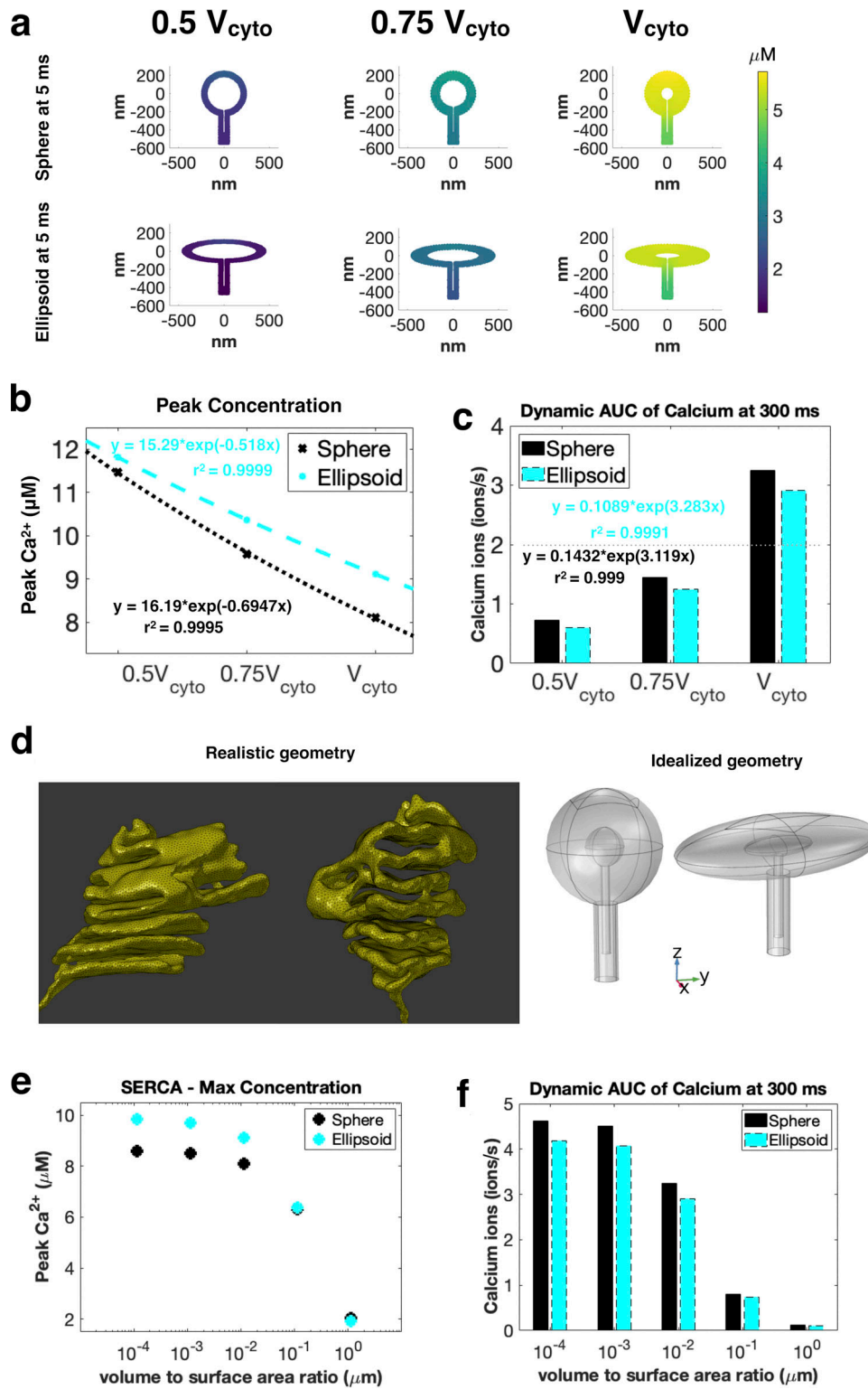


**Figure 5. Increasing SpApp volume reduces accumulated calcium and SpApp volume-to-surface area modulates its ability to act as a sink.** (a) Calcium dynamics depends on the size of SpApp; decreasing cytoplasmic volume by increasing SpApp size results in a smaller calcium concentration when compared with a larger spine volume with smaller SpApp. The effect of SpApp size on the temporal dynamics of calcium is seen in the (b) peak values and (c) AUCs of calcium. Increasing SpApp volume (decreasing spine volume) decreases calcium concentration in the spine (a and c) but leads to higher peak concentrations (b). For both geometries, the peak calcium concentration increases for decreasing volume, and can be fit to exponential curves. (d) While we are used idealized geometries for both the spine and SpApp, in reality, the SpApp has a complex, helicoidal structure. We investigate this realistic geometry by changing the  $n_{SpApp}$  contribution in the SERCA flux equation. We see that increasing  $n_{SpApp}$  makes SERCA more effective, leading to lower peak concentrations (e) and lower AUC (f). However, we see that as we decrease  $n_{SpApp}$ , the change in peak concentration and AUC plateaus, representing highly inefficient SERCA pumps. cyto, cytoplasm.

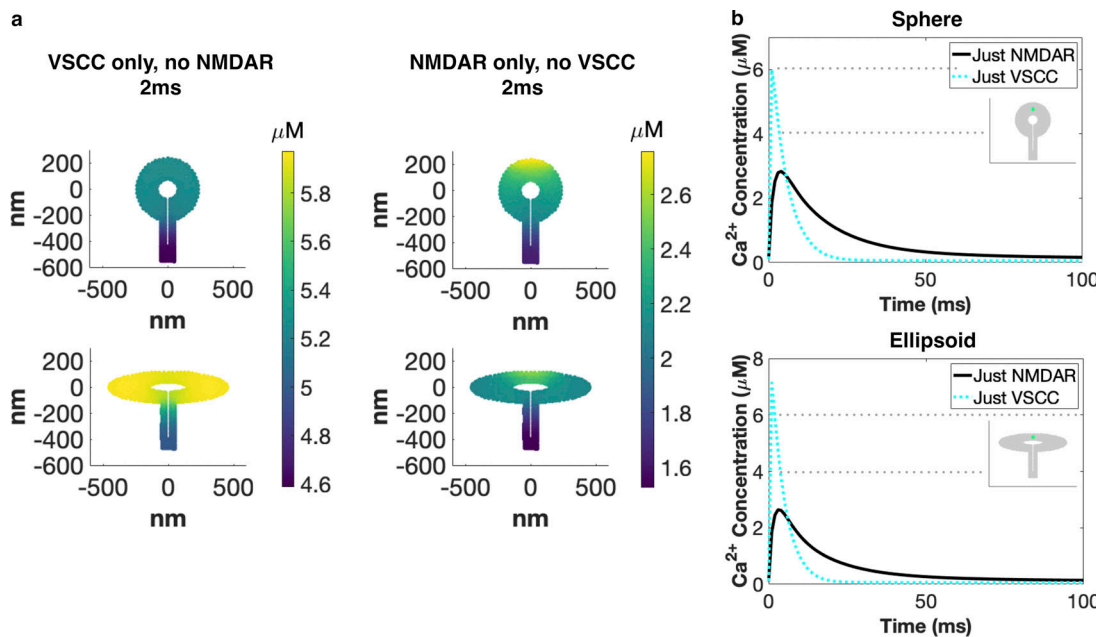


**Figure 6. Localization of membrane fluxes alters the spatiotemporal dynamics of calcium.** (a) Spatial dynamics at 2 ms for spherical and ellipsoidal spines with only one of VSCC or NMDAR as the calcium source. When the main calcium source is the VSCC, we see a more uniform concentration with the main gradient between the spine head and spine neck. When the NMDAR is the main calcium source, we see a large spatial gradient with a higher concentration at the PSD, because the NMDAR is localized to the PSD. (b) Temporal dynamics for spherical and ellipsoidal spines with either the VSCC or NMDAR as the calcium source. Temporal dynamics clearly show that VSCCs act on a faster timescale and have a higher peak calcium when compared with the NMDARs. However, NMDAR influx leads to a more prolonged calcium transient.

An intriguing feature of the SpApp in particular (Fig. 5 d; Wu et al., 2017) and the ER in general (Nixon-Abell et al., 2016) is the large surface-to-volume ratio occupied by this organelle. Therefore, we next considered the effect of the volume-to-surface area ratio ( $n$ ; given in units of length) of the SpApp (Fig. 5, d-f). We modeled the boundary flux on the SpApp membrane such that this flux is proportional to  $n_{\text{SpApp}}$  (volume-to-surface area ratio for the SpApp). As a result, when we increase the “volume” of the SpApp by increasing  $n_{\text{SpApp}}$ , calcium flux into the SpApp will increase. We noticed that at lower  $n_{\text{SpApp}}$  values, the peak calcium concentration and to a less obvious extent the AUC (Fig. 5, e and f) plateau but decrease substantially at larger  $n_{\text{SpApp}}$  values.

From these observations, we conclude that the SpApp acts as a physical and spatial buffer for calcium dynamics by regulating the timescale through surface to volume regulation in the interior of the spine. The SpApp acts as a calcium sink in the timescale of interest (Fifková et al., 1983; Fifková, 1985; Jedlicka et al., 2008), and in the absence of the SpApp, the only way to remove calcium from this system is through CBPs and pumps. Furthermore, since the SpApp has been known to grow and retract from the dendritic spine in response to stimuli (Deller et al., 2006), regulation of SpApp surface area can also allow for rescaling calcium dynamics in the spine (Wilson et al., 1983).

#### Spatial distribution of membrane fluxes governs calcium dynamics supralinearly in dendritic spines

The density of VSCCs and number of NMDARs that open in response to stimuli in dendritic spines varies (Sabatini and

Svoboda, 2000). One of the primary determinants of calcium dynamics in the spine is the various membrane fluxes, because these fluxes serve as sources and sinks at the PM and sinks at the SpApp membrane. We investigated the effect of the spatial distribution of membrane fluxes on calcium dynamics in the dendritic spine by considering either only NMDARs or VSCCs as the calcium source (Fig. 6). We observed that if only NMDAR activity was present, then calcium concentration was high in the PSD region due to the localization of NMDARs to the PSD but the overall calcium concentration was small regardless of the spine head shape (Fig. 6 a). However, if only VSCCs were active, then the spatial gradient of calcium is mainly between the spine head and spine neck (Fig. 6 a). The temporal dynamics are also affected by the receptor and channel distributions (Fig. 6 b). With only VSCCs present, there is a larger calcium peak, but with faster decay. With only NMDARs, we observe a lower calcium peak concentration but a prolonged transient. Therefore, membrane flux distribution can impact the spatial and temporal dynamics of calcium in a nonlinear manner. This agrees with experimental results stating that the various calcium sources behave supralinearly (Yuste and Denk, 1995) and a balance between various calcium fluxes is required for tightly regulating calcium concentrations in these small volumes.

#### Calcium buffers and diffusion couple to alter calcium spatiotemporal dynamics

Due to the vast number of buffers that are known to affect calcium dynamics, we investigated the effect of four different buffer conditions: (i) both fixed membrane-bound buffers and

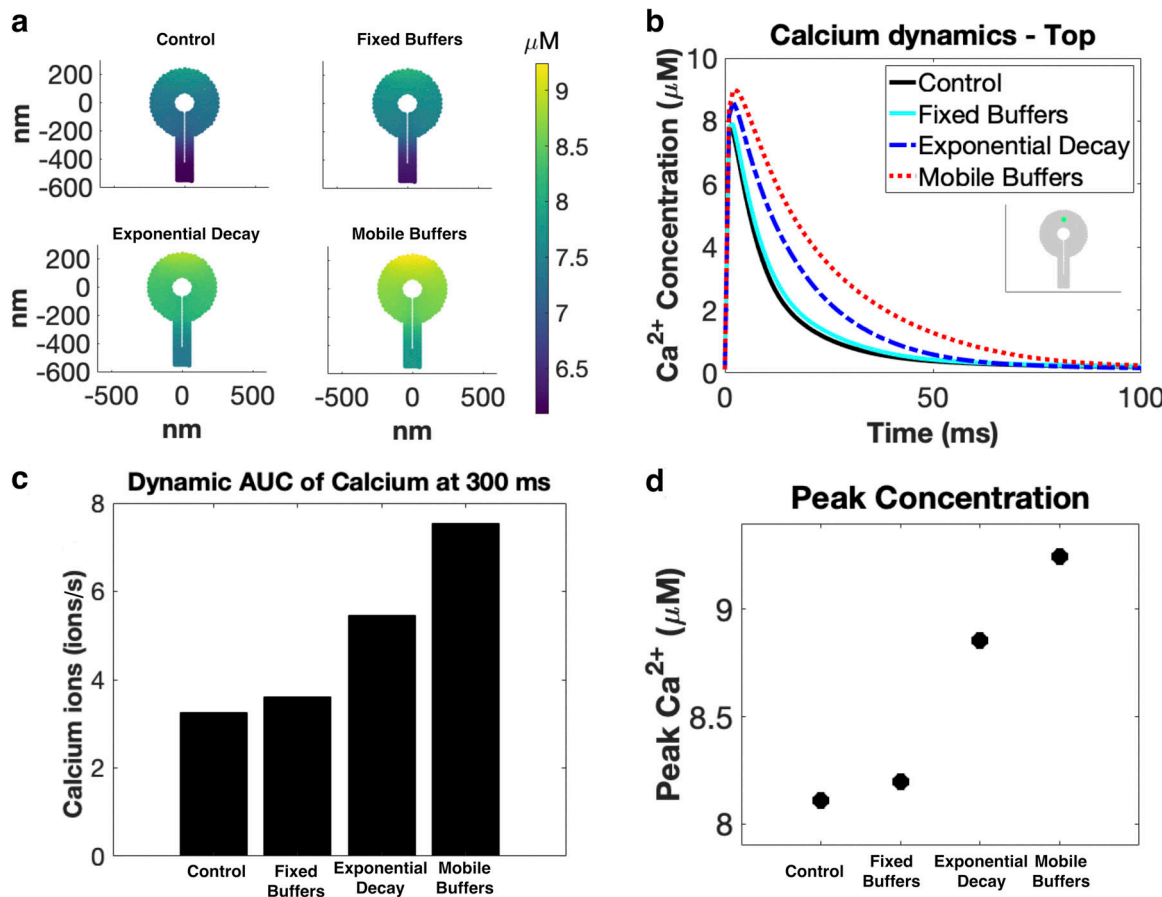


**Figure 7. Calcium buffers and CBPs modify all aspects of calcium dynamics.** (a) Spatial dynamics at 2 ms for spherical spines with different buffer conditions: control (with both fixed and mobile buffers), only fixed buffers, only mobile buffers, and a lumped exponential decay. While all buffer cases show relatively similar peak concentrations (d), all other quantifications show that buffer type greatly impacts the calcium transient decay time (a-c). Temporal dynamics (b) show that the control and fixed buffer cases have much faster decay, which translates into lower AUC values (c).

mobile cytosolic buffers (control), (ii) fixed buffers localized to the membrane, (iii) mobile buffers in the cytoplasm, and (iv) a uniform exponential decay applied across the whole cytoplasm (Figs. 7 and S9). We observe similar spatial dynamics for all buffer types (Fig. 7 a), but temporal dynamics differ greatly (Fig. 7 b) and, as a result, alter accumulated calcium (Fig. 7 c). We see that the decay behavior of calcium, and therefore total calcium, is highly dependent on buffer type. Peak calcium follows the same trend as AUC, with mobile buffers having the highest calcium concentrations and total calcium, then exponential decay, fixed buffers, and finally the control. We also consider how reaction dynamics versus diffusion rate govern calcium dynamics because buffer dynamics and diffusion rates of calcium are coupled (Yuste et al., 2000). We varied the diffusion rate of calcium and the concentration of mobile buffers to quantify how calcium dynamics are reaction or diffusion controlled (Fig. 8). We see that diffusion controls the spatial gradient seen within the spine (Fig. 8 a), while mobile buffer concentration controls the lifetime of the calcium transient (Fig. 8 b). Combining these effects, we see that the buffer concentration variation has the greatest effect at lower diffusion rates (bottom row of Fig. 8, a and b, and Fig. 8 c). The peak concentration of calcium is almost entirely dependent on the diffusion rate (Fig. 8 d). Therefore,

based on the high diffusion rate of  $\text{Ca}^{2+}$  reported in the literature, we expect the system to be in a diffusion-dominated regimen.

## Discussion

Calcium is a fundamental player in both neuronal (cellular) and neural (systems) functionality (Siesjö, 1990; Keener and Sneyd, 1998; Yuste, 2010). Compartmentalized by dendritic spines, calcium has a vital role in triggering signaling pathways for long-term potentiation, long-term depression, synaptic plasticity, and other processes associated with learning and memory formation (Rangamani et al., 2016). However, while dendritic spines are known to form functional sub-compartments, it is less understood how this specialized compartmentalization impacts calcium dynamics (Yuste et al., 2000). In this study, we explored the intricate relationship between calcium dynamics and the shape and size of dendritic spine structures. We found that while the relationship between spine geometry and calcium dynamics is quite complicated (Hering and Sheng, 2001; Rochelefort and Konnerth, 2012; Berry and Nedivi, 2017), some general conclusions can be drawn from our study.

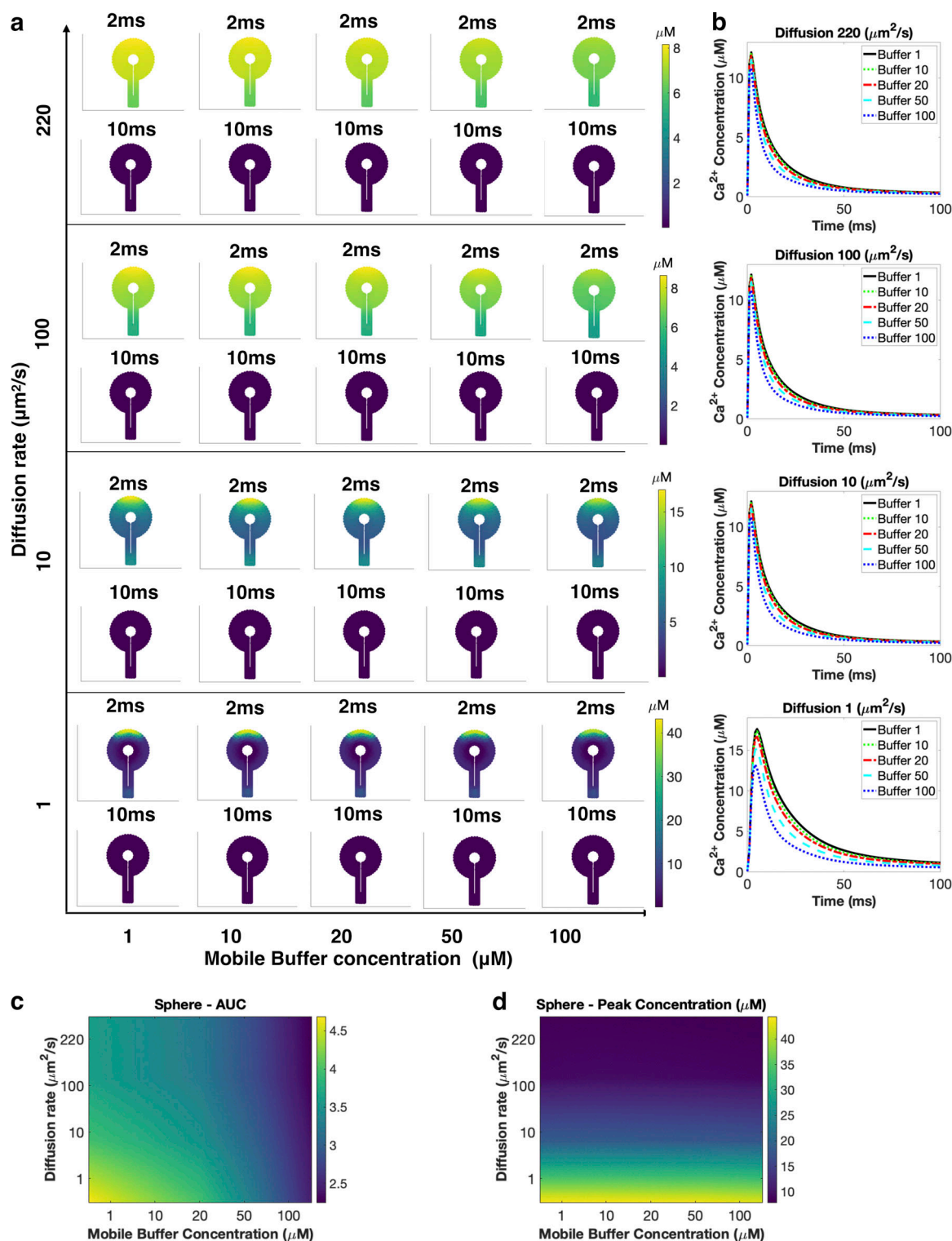


**Figure 8. Calcium diffusion rates control spatial gradients of calcium while buffer concentrations control transient decay dynamics.** **(a)** Spatial dynamics at 2 ms and 10 ms for a spherical spine. We varied the diffusion coefficient and the mobile buffer concentration. Based on this phase diagram, the diffusion coefficient dictates the range of the spatial gradient of calcium, while buffer binding rate influences the lifetime of the spatial gradient. **(b)** Temporal calcium dynamics at the top of the spherical spine. The temporal dynamics show that the concentration of mobile buffer affects the lifetime of the calcium transient, as expected. **(c)** AUC shows that lower mobile buffer concentration and lower diffusion rates leads to higher levels of total calcium. **(d)** Peak concentration is primarily determined by the diffusion rate of calcium and is almost independent of mobile buffer concentration.

First, the volume-to-surface ratio, rather than the shape and size itself, seems to have a dramatic effect on spine calcium (Figs. 2, 3, 4, and 5). Of course, the volume-to-surface ratio itself can be dramatically altered by size, shape, and internal organization as a many-to-one function. Then, we can think of the ultrastructural organization of the dendritic spine (Spacek and Harris, 1997) as perhaps “optimized” to not only increase contacts with neighboring axons and neural circuit connection (Yuste and Denk, 1995; Yuste et al., 2000; Yuste, 2010) but also tune this volume-to-surface ratio dynamically (Murakoshi and Yasuda, 2012). This volume-to-surface ratio coupling further highlights the complex relationship between spatial sources and sinks of calcium, which becomes apparent when the distance between the spine PM and internal organelle becomes quite small. We note that in our model, we assume constant pump density, which highlights the volume-to-surface area ratios between various shapes (Matsuzaki et al., 2001; Noguchi et al., 2005). Experimental results have already shown different behavior in large versus small dendritic spines (Paulin et al., 2016), and additional studies on dendritic spine geometry have shown that stable, mature spines are usually larger spines that tend toward mushroom shapes as they grow around adjoining axons and are more likely to have a SpApp (Spacek and Harris, 1997). In comparison, younger, less stable spines tend to be smaller and more spherical (Spacek and Harris, 1997; Berry and Nedivi, 2017). Therefore, we predict that spine size and SpApp presence are coupled to control calcium dynamics. This result should be investigated further, in particular to make predictions on why stable spines tend to be larger and mushroom shaped. The inverse relationship between the volume-to-surface ratio that we found and a possible exponential relationship suggest a potential limiting mechanism for maintaining homeostasis of synaptic potentiation (Lee et al., 2010, 2012; Béique et al., 2011; Turrigiano, 2011). By altering the spine size dynamically (Murakoshi and Yasuda, 2012) and the presence and absence of the SpApp dynamically (Deller et al., 2006), spines could maintain their optimal range of synaptic function (Lee et al., 2010, 2012; Béique et al., 2011; Turrigiano, 2011).

Second, localization of membrane fluxes alters calcium transients (Figs. 5 and 6). These fluxes, which serve as boundary conditions, can be altered by changing the density and distribution of calcium sources and sinks. This idea is consistent with how calcium signal localization is a result of tuning the distance between sources and sinks (Augustine et al., 2003). We show here that in addition to distance, the strength of the fluxes is important. Thus, in various disease states that impact the distribution or strength of membrane components, we predict atypical spatial calcium gradients are possible that could impact downstream signaling pathways. For example, NMDAR dysfunction, whether leading to increased or decreased functionality, can potentially lead to central nervous system diseases such as stroke, Huntington’s disease, or schizophrenia (Zhou and Sheng, 2013).

Finally, the role buffers play in modulating calcium transients is not only by changing the decay time as previously thought but also by tuning the membrane fluxes, especially in the case of fixed buffers (Figs. 7 and 8; Higley and Sabatini, 2012;

Matthews and Dietrich, 2015). Again, the timescale that we see is a combination of rate alterations at the membrane and rate alterations in the volume resulting in broader control of calcium dynamics. The crowded environment within the spine head also has consequences for calcium diffusion, and while it is possible for calcium to diffuse through a crowded space, particularly in the PSD, the exact mechanisms of such transport remain unclear (Santamaria et al., 2006; Hotulainen and Hoogenraad, 2010; Byrne et al., 2011). Thus, our study highlights the need for connecting biophysical features of the spine and molecule localization to the dynamics of calcium (Fig. 1).

We also note that our model has certain limitations. In particular, within the crowded environment of the dendritic spine cytoplasm is an abundance of actin, which has previously been shown to have the potential to create cytosolic flow through contraction following spine activation, leading to faster calcium diffusion (Holcman et al., 2004). We do not address this spine contraction in this model, but actin contributions are a focus of ongoing research in our group. While we touched upon the role of diffusion and CBPs, we also acknowledge that much work remains to be done on the true impact of the dense actin network and crowded environment within dendritic spines in regulating these processes (Ouyang et al., 2005). In addition, we modeled isolated spines, but the width of the spine neck has been shown as an important determinant of calcium dynamics when comparing larger and smaller spines (Noguchi et al., 2005; Arellano et al., 2007; Araya et al., 2014) and could play into communication to the dendrite. It is also possible that stochastic modeling will give better quantitative insights without altering the underlying physics (Kotaleski and Blackwell, 2010; Bartol et al., 2015b; Voorsluys et al., 2019). The development of a combined stochastic-deterministic model can help combine these two regimes to address the fundamental physics that occurs in these small systems with complex membrane dynamics and few molecule situations.

Despite these shortcomings, we have identified several key features of the relationship between dendritic spine geometry and calcium dynamics. Current models of synaptic weight updates use calcium as the determinant for the synaptic weight vector and the learning rate (Malenka et al., 1988; Cummings et al., 1996; Shouval et al., 2002; Yeung et al., 2004). Here, we show that calcium in a spine, even in short timescales, is a function of geometry, ultrastructure, and buffers. Based on these insights, we speculate on what the biophysical features of the spine mean for neural systems-level functionality. It has long been considered that a neural circuit level model of synaptic weight updates can be informed by the calcium transients in the synapse. As a result, weighting functions have been proposed that consider calcium dynamics (Cummings et al., 1996; Shouval et al., 2002; Yeung et al., 2004), and these functions have been used to connect biophysical features of NMDARs to synaptic weight updates in models of spike time-dependent plasticity (STDP; Sejnowski, 1977; Song et al., 2000; Izhikevich, 2007; Bush and Jin, 2012; Standage et al., 2014). We now propose that the calcium transient is explicitly a function of the spine volume-to-surface area, ultrastructure, and buffers, and that the calcium functions that inform the synaptic weight vectors and synaptic

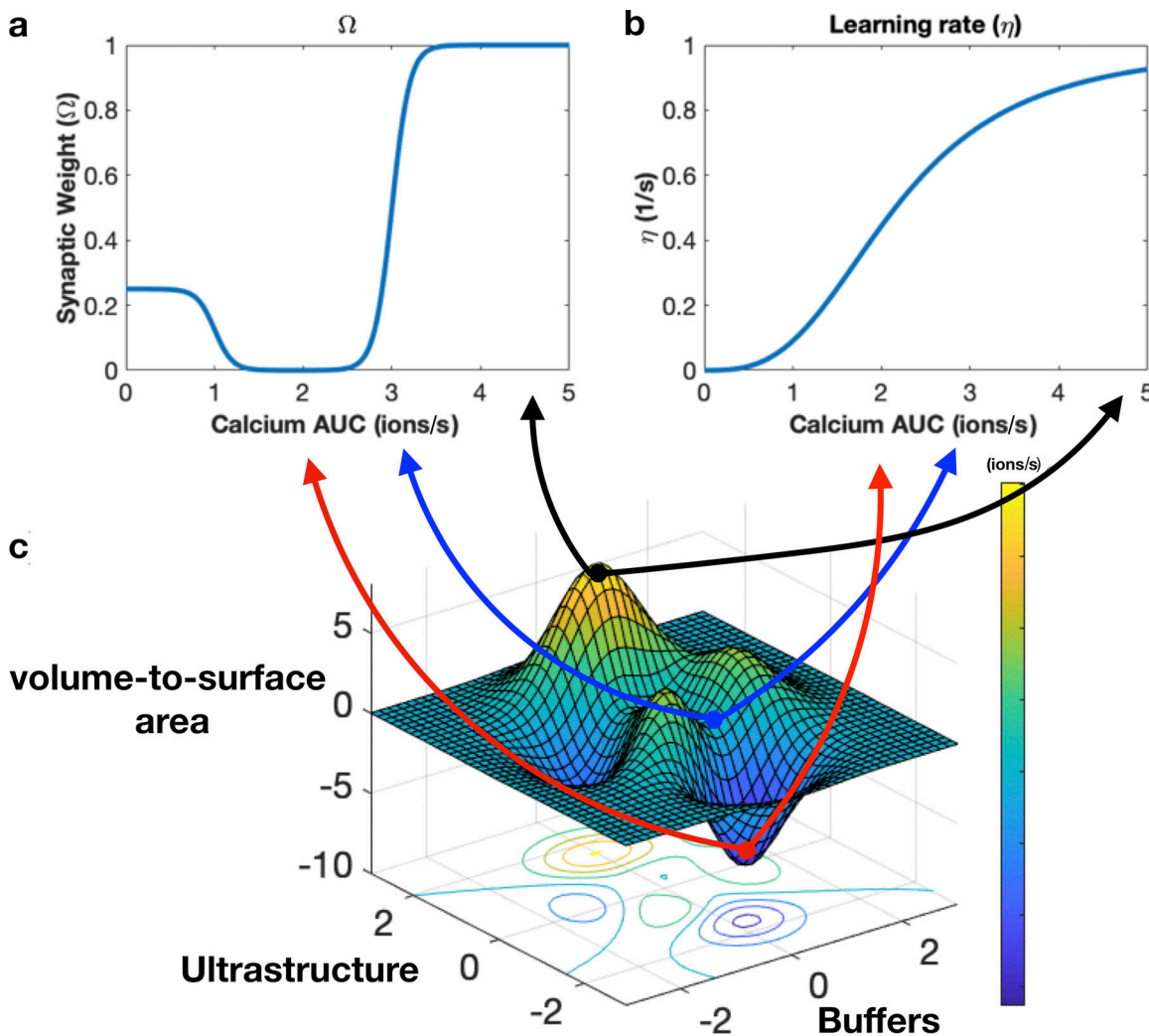


**Figure 9. Biophysical factors can impact synaptic weights through calcium dynamics.** (a) Synaptic weight can be calculated from calcium dynamics (Shouval et al., 2002). We plot changes in synaptic weight due to calcium quantified through accumulated calcium. (b) Calcium dynamics also dictate the learning rate of the spine. (c) Qualitative representation of the effects of calcium AUC on synaptic weight and learning rate. Using our model, we can map how various factors governing calcium dynamics influence both synaptic weights and learning rates of dendritic spines. This surface plot visualizes how three different factors (volume to surface area ratio, ultrastructure, and calcium buffers) couple to influence calcium AUC (color bar) that feeds back into synaptic weight changes and learning rates.

Downloaded from [http://jgpess.org/jgp/article-pdf/151/8/1017/1800492/jgp\\_201812261.pdf](http://jgpress.org/jgp/article-pdf/151/8/1017/1800492/jgp_201812261.pdf) by guest on 08 February 2026

learning rate (Fig. 9) must be updated to consider such geometric information. We anticipate that such new models can give us better insight into the neural circuitry of the brain and also better inform bioinspired engineering of neuromorphic circuits (Cruz-Albrecht et al., 2012). We also acknowledge that much work remains to be done in connecting the spatial signaling aspects in postsynaptic spines with neural circuit behavior but hope that this work will inspire more multiscale modeling efforts in this field. The spatial aspects of calcium dynamics are also fundamental toward understanding the downstream dynamics of critical molecules such as calcium/calmodulin-dependent protein kinase II (CaMKII), the small RhoGTPases (Cdc42, Rho, and Rac), and subsequently actin dynamics in dendritic spine remodeling (Oertner and Matus, 2005; Murakoshi and Yasuda, 2012; Miermans et al., 2017; Ohadi and Rangamani, 2019 *Preprint*; Ohadi et al., 2019 *Preprint*; Yasuda et al., 2003; Rangamani et al., 2016; Yasuda, 2017). Going

beyond single spine dynamics, the propagation of the downstream mechanochemical activity to neighboring spines is a key step toward integrating single spine behavior to multiple spines, across the dendrite, and ultimately the whole cell (Majewska et al., 2000; Bloodgood and Sabatini, 2005; Herz et al., 2006; Schmidt et al., 2007; Yasuda, 2017). Thus, we posit that accounting for the spatial and physical aspects of calcium dynamics is the first step toward deciphering the complex shape-function relationships of dendritic spines.

## Acknowledgments

We thank various members of the Rangamani Lab for valuable discussion, Mariam Ordyan for manuscript review, and Professor Brenda Bloodgood and Evan Campbell for their expertise. We thank Professor Pietro De Camilli and his laboratory for supplying images used to construct the mesh seen in Fig. 5 d.

This work was supported by the University of California, San Diego Interfaces Graduate Training Program and a San Diego Fellowship, Air Force Office of Scientific Research (AFOSR) Multidisciplinary University Research Initiative (MURI) grant FA9550-18-1-0051 (M. Bell, P. Rangamani, and T. Sejnowski), and the National Institutes of Health (grant T32EB009380).

The authors declare no competing financial interests.

Author contributions: M. Bell and P. Rangamani conceived the project. M. Bell conducted all the simulations. All authors conducted data analysis and contributed to writing the manuscript. M. Bell made all the figures.

José D. Faraldo-Gómez served as editor.

Submitted: 26 September 2018

Revised: 10 May 2019

Accepted: 17 June 2019

## References

Araya, R., T.P. Vogels, and R. Yuste. 2014. Activity-dependent dendritic spine neck changes are correlated with synaptic strength. *Proc. Natl. Acad. Sci. USA*. 111:E2895–E2904. <https://doi.org/10.1073/pnas.1321869111>

Arellano, J.I., R. Benavides-Piccione, J. Defelipe, and R. Yuste. 2007. Ultrastructure of dendritic spines: correlation between synaptic and spine morphologies. *Front. Neurosci.* 1:131–143. [https://doi.org/10.3389/neuro\\_01.11.010.2007](https://doi.org/10.3389/neuro_01.11.010.2007)

Atay, O., and J.M. Skotheim. 2017. Spatial and temporal signal processing and decision making by MAPK pathways. *J. Cell Biol.* 216:317–330. <https://doi.org/10.1083/jcb.201609124>

Augustine, G.J., F. Santamaria, and K. Tanaka. 2003. Local calcium signaling in neurons. *Neuron*. 40:331–346. [https://doi.org/10.1016/S0896-6273\(03\)00639-1](https://doi.org/10.1016/S0896-6273(03)00639-1)

Bartol, T.M. Jr., C. Bromer, J. Kinney, M.A. Chirillo, J.N. Bourne, K.M. Harris, and T.J. Sejnowski. 2015a. Nanoconnectomic upper bound on the variability of synaptic plasticity. *eLife*. 4:e10778. <https://doi.org/10.7554/eLife.10778>

Bartol, T.M., D.X. Keller, J.P. Kinney, C.L. Bajaj, K.M. Harris, T.J. Sejnowski, and M.B. Kennedy. 2015b. Computational reconstitution of spine calcium transients from individual proteins. *Front. Synaptic Neurosci.* 7:17. <https://doi.org/10.3389/fnsyn.2015.00017>

Basak, R., and R. Narayanan. 2018. Active dendrites regulate the spatiotemporal spread of signaling microdomains. *PLOS Comput. Biol.* 14: e1006485. <https://doi.org/10.1371/journal.pcbi.1006485>

Basnayake, K., E. Korkotian, and D. Holcman. 2018. Fast calcium transients in neuronal spines driven by extreme statistics. *bioRxiv*. doi:10.1101/290734 (Preprint posted April 8, 2018)

Béique, J.-C., Y. Na, D. Kuhl, P.F. Worley, and R.L. Huganir. 2011. Arc-dependent synapse-specific homeostatic plasticity. *Proc. Natl. Acad. Sci. USA*. 108:816–821. <https://doi.org/10.1073/pnas.1017914108>

Berry, K.P., and E. Nedivi. 2017. Spine dynamics: are they all the same? *Neuron*. 96:43–55. <https://doi.org/10.1016/j.neuron.2017.08.008>

Bloodgood, B.L., and B.L. Sabatini. 2005. Neuronal activity regulates diffusion across the neck of dendritic spines. *Science*. 310:866–869. <https://doi.org/10.1126/science.1114816>

Bourne, J.N., and K.M. Harris. 2008. Balancing structure and function at hippocampal dendritic spines. *Annu. Rev. Neurosci.* 31:47–67. <https://doi.org/10.1146/annurev.neuro.31.060407.125646>

Bush, D., and Y. Jin. 2012. Calcium control of triphasic hippocampal STDP. *J. Comput. Neurosci.* 33:495–514. <https://doi.org/10.1007/s10827-012-0397-5>

Byrne, M.J., M.N. Waxham, and Y. Kubota. 2011. The impacts of geometry and binding on CaMKII diffusion and retention in dendritic spines. *J. Comput. Neurosci.* 31:1–12. <https://doi.org/10.1007/s10827-010-0293-9>

Calizo, R.C., A. Ron, M. Hu, S. Bhattacharya, W.G.M. Janssen, J. Hone, S. Scarlata, P. Rangamani, and R. Iyengar. 2017. Curvature regulates subcellular organelle location to control intracellular signal propagation. *bioRxiv*. doi:10.1101/161950 (Preprint posted July 11, 2017)

Clapham, D.E. 1995. Calcium signaling. *Cell*. 80:259–268. [https://doi.org/10.1016/0092-8674\(95\)90408-5](https://doi.org/10.1016/0092-8674(95)90408-5)

Clapham, D.E. 2007. Calcium signaling. *Cell*. 131:1047–1058. <https://doi.org/10.1016/j.cell.2007.11.028>

Cruz-Albrecht, J.M., M.W. Yung, and N. Srinivasa. 2012. Energy-efficient neuron, synapse and STDP integrated circuits. *IEEE Trans. Biomed. Circuits Syst.* 6:246–256. <https://doi.org/10.1109/TBCAS.2011.2174152>

Cugno, A., T.M. Bartol, T.J. Sejnowski, R. Iyengar, and P. Rangamani. 2018. Geometric principles of second messenger dynamics in dendritic spines. *bioRxiv*. doi:10.1101/444489 (Preprint posted October 20, 2018)

Cummings, J.A., R.M. Mulkey, R.A. Nicoll, and R.C. Malenka. 1996. Ca<sup>2+</sup> signaling requirements for long-term depression in the hippocampus. *Neuron*. 16:825–833. [https://doi.org/10.1016/S0896-6273\(00\)80102-6](https://doi.org/10.1016/S0896-6273(00)80102-6)

Deller, T., C. Bas Orth, A. Vlachos, T. Merten, D. Del Turco, D. Dehn, P. Mundel, and M. Frotscher. 2006. Plasticity of synaptopodin and the spine apparatus organelle in the rat fascia dentata following entorhinal cortex lesion. *J. Comp. Neurol.* 499:471–484. <https://doi.org/10.1002/cne.21103>

Denk, W., R. Yuste, K. Svoboda, and D.W. Tank. 1996. Imaging calcium dynamics in dendritic spines. *Curr. Opin. Neurobiol.* 6:372–378. [https://doi.org/10.1016/S0959-4388\(96\)80122-X](https://doi.org/10.1016/S0959-4388(96)80122-X)

Fifková, E. 1985. A possible mechanism of morphometric changes in dendritic spines induced by stimulation. *Cell. Mol. Neurobiol.* 5:47–63. <https://doi.org/10.1007/BF00711085>

Fifková, E., J.A. Markham, and R.J. Delay. 1983. Calcium in the spine apparatus of dendritic spines in the dentate molecular layer. *Brain Res.* 266: 163–168. [https://doi.org/10.1016/0006-8993\(83\)91322-7](https://doi.org/10.1016/0006-8993(83)91322-7)

Futagi, D., and K. Kitano. 2015. Ryanodine-receptor-driven intracellular calcium dynamics underlying spatial association of synaptic plasticity. *J. Comput. Neurosci.* 39:329–347. <https://doi.org/10.1007/s10827-015-0579-z>

Gallimore, A.R., A.R. Aricescu, M. Yuzaki, and R. Calinescu. 2016. A computational model for the ampa receptor phosphorylation master switch regulating cerebellar long-term depression. *PLOS Comput. Biol.* 12: e1004664. <https://doi.org/10.1371/journal.pcbi.1004664>

Gorman, R.P., and T.J. Sejnowski. 1988. Analysis of hidden units in a layered network trained to classify sonar targets. *Neural Netw.* 1:75–89. [https://doi.org/10.1016/0893-6080\(88\)90023-8](https://doi.org/10.1016/0893-6080(88)90023-8)

Griffith, T., K. Tsaneva-Atanasova, and J.R. Mellor. 2016. Control of ca2+ influx and calmodulin activation by sk-channels in dendritic spines. *PLOS Comput. Biol.* 12:e1004949. <https://doi.org/10.1371/journal.pcbi.1004949>

Heinrich, R., B.G. Neel, and T.A. Rapoport. 2002. Mathematical models of protein kinase signal transduction. *Mol. Cell.* 9:957–970. [https://doi.org/10.1016/S1097-2765\(02\)00528-2](https://doi.org/10.1016/S1097-2765(02)00528-2)

Hering, H., and M. Sheng. 2001. Dendritic spines: structure, dynamics and regulation. *Nat. Rev. Neurosci.* 2:880–888. <https://doi.org/10.1038/35104061>

Herz, A.V., T. Gollisch, C.K. Machens, and D. Jaeger. 2006. Modeling single-neuron dynamics and computations: a balance of detail and abstraction. *Science*. 314:80–85. <https://doi.org/10.1126/science.1127240>

Higley, M.J., and B.L. Sabatini. 2012. Calcium signaling in dendritic spines. *Cold Spring Harb. Perspect. Biol.* 4:a005686. <https://doi.org/10.1101/cshperspect.a005686>

Holbro, N., A. Grunditz, and T.G. Oertner. 2009. Differential distribution of endoplasmic reticulum controls metabotropic signaling and plasticity at hippocampal synapses. *Proc. Natl. Acad. Sci. USA*. 106:15055–15060. <https://doi.org/10.1073/pnas.0905110106>

Holcman, D., Z. Schuss, and E. Korkotian. 2004. Calcium dynamics in dendritic spines and spine motility. *Biophys. J.* 87:81–91. <https://doi.org/10.1529/biophysj.103.035972>

Holmes, W.R. 1990. Is the function of dendritic spines to concentrate calcium? *Brain Res.* 519:338–342. [https://doi.org/10.1016/0006-8993\(90\)90098-V](https://doi.org/10.1016/0006-8993(90)90098-V)

Hoogland, T.M., and P. Saggau. 2004. Facilitation of L-type Ca<sup>2+</sup> channels in dendritic spines by activation of β2 adrenergic receptors. *J. Neurosci.* 24: 8416–8427. <https://doi.org/10.1523/JNEUROSCI.1677-04.2004>

Hotulainen, P., and C.C. Hoogenraad. 2010. Actin in dendritic spines: connecting dynamics to function. *J. Cell Biol.* 189:619–629. <https://doi.org/10.1083/jcb.201003008>

Hu, E., A. Mergenthal, C.S. Bingham, D. Song, J.-M. Bouteiller, and T.W. Berger. 2018. A glutamatergic spine model to enable multi-scale modeling of nonlinear calcium dynamics. *Front. Comput. Neurosci.* 12:58. <https://doi.org/10.3389/fncom.2018.00058>

Izhikevich, E.M. 2007. Solving the distal reward problem through linkage of STDP and dopamine signaling. *Cereb. Cortex*. 17:2443–2452. <https://doi.org/10.1093/cercor/bhl152>

Jaffe, D.B., S.A. Fisher, and T.H. Brown. 1994. Confocal laser scanning microscopy reveals voltage-gated calcium signals within hippocampal dendritic spines. *J. Neurobiol.* 25:220–233. <https://doi.org/10.1002/neu.480250303>

Jahr, C.E., and C.F. Stevens. 1993. Calcium permeability of the N-methyl-D-aspartate receptor channel in hippocampal neurons in culture. *Proc. Natl. Acad. Sci. USA* 90:11573–11577. <https://doi.org/10.1073/pnas.90.24.11573>

Jedlicka, P., A. Vlachos, S.W. Schwarzacher, and T. Deller. 2008. A role for the spine apparatus in LTP and spatial learning. *Behav. Brain Res.* 192:12–19. <https://doi.org/10.1016/j.bbr.2008.02.033>

Kasai, H., M. Fukuda, S. Watanabe, A. Hayashi-Takagi, and J. Noguchi. 2010. Structural dynamics of dendritic spines in memory and cognition. *Trends Neurosci.* 33:121–129. <https://doi.org/10.1016/j.tins.2010.01.001>

Keener, J.P., and J. Sneyd. 1998. *Mathematical Physiology*. Vol. 1. Springer-Verlag, New York. <https://doi.org/10.1007/b98841>

Knott, G.W., A. Holtmaat, L. Wilbrecht, E. Welker, and K. Svoboda. 2006. Spine growth precedes synapse formation in the adult neocortex *in vivo*. *Nat. Neurosci.* 9:1117–1124. <https://doi.org/10.1038/nn1747>

Koch, C., and A. Zador. 1993. The function of dendritic spines: devices subserving biochemical rather than electrical compartmentalization. *J. Neurosci.* 13:413–422. <https://doi.org/10.1523/JNEUROSCI.13-02-00413.1993>

Kotaleski, J.H., and K.T. Blackwell. 2010. Modelling the molecular mechanisms of synaptic plasticity using systems biology approaches. *Nat. Rev. Neurosci.* 11:239–251. <https://doi.org/10.1038/nrn2807>

Kuwajima, M., J. Spacek, and K.M. Harris. 2013. Beyond counts and shapes: studying pathology of dendritic spines in the context of the surrounding neuropil through serial section electron microscopy. *Neuroscience*. 251: 75–89. <https://doi.org/10.1016/j.neuroscience.2012.04.061>

Lee, K.F., C. Soares, and J.-C. Béique. 2012. Examining form and function of dendritic spines. *Neural Plast.* 2012:704103. <https://doi.org/10.1155/2012/704103>

Lee, M.-C., R. Yasuda, and M.D. Ehlers. 2010. Metaplasticity at single glutamatergic synapses. *Neuron*. 66:859–870. <https://doi.org/10.1016/j.neuron.2010.05.015>

Lee, S.-J.R., Y. Escobedo-Lozoya, E.M. Szatmari, and R. Yasuda. 2009. Activation of CaMKII in single dendritic spines during long-term potentiation. *Nature*. 458:299–304. <https://doi.org/10.1038/nature07842>

Loewenstein, Y., and H. Sompolinsky. 2003. Temporal integration by calcium dynamics in a model neuron. *Nat. Neurosci.* 6:961–967. <https://doi.org/10.1038/nn1109>

Majewska, A., A. Tashiro, and R. Yuste. 2000. Regulation of spine calcium dynamics by rapid spine motility. *J. Neurosci.* 20:8262–8268. <https://doi.org/10.1523/JNEUROSCI.20-22-08262.2000>

Malenka, R.C., J.A. Kauer, R.S. Zucker, and R.A. Nicoll. 1988. Postsynaptic calcium is sufficient for potentiation of hippocampal synaptic transmission. *Science*. 242:81–84. <https://doi.org/10.1126/science.2845577>

Matsuzaki, M., G.C. Ellis-Davies, T. Nemoto, Y. Miyashita, M. Iino, and H. Kasai. 2001. Dendritic spine geometry is critical for AMPA receptor expression in hippocampal CA1 pyramidal neurons. *Nat. Neurosci.* 4: 1086–1092. <https://doi.org/10.1038/nn736>

Matthews, E.A., and D. Dietrich. 2015. Buffer mobility and the regulation of neuronal calcium domains. *Front. Cell. Neurosci.* 9:48. <https://doi.org/10.3389/fncel.2015.00048>

Matthews, E.A., S. Schoch, and D. Dietrich. 2013. Tuning local calcium availability: cell-type-specific immobile calcium buffer capacity in hippocampal neurons. *J. Neurosci.* 33:14431–14445. <https://doi.org/10.1523/JNEUROSCI.4118-12.2013>

Mattson, M.P., F.M. LaFerla, S.L. Chan, M.A. Leisring, P.N. Shepel, and J.D. Geiger. 2000. Calcium signaling in the ER: its role in neuronal plasticity and neurodegenerative disorders. *Trends Neurosci.* 23:222–229. [https://doi.org/10.1016/S0166-2236\(00\)01548-4](https://doi.org/10.1016/S0166-2236(00)01548-4)

Maurya, M.R., and S. Subramaniam. 2007. A kinetic model for calcium dynamics in RAW 264.7 cells: 1. Mechanisms, parameters, and sub-population variability. *Biophys. J.* 93:709–728. <https://doi.org/10.1529/biophysj.106.097469>

Means, S., A.J. Smith, J. Shepherd, J. Shadid, J. Fowler, R.J. Wojcikiewicz, T. Mazel, G.D. Smith, and B.S. Wilson. 2006. Reaction diffusion modeling of calcium dynamics with realistic ER geometry. *Biophys. J.* 91:537–557. <https://doi.org/10.1529/biophysj.105.075036>

Miermans, C.A., R.P. Kusters, C.C. Hoogenraad, and C. Storm. 2017. Biophysical model of the role of actin remodeling on dendritic spine morphology. *PLoS One.* 12:e0170113. <https://doi.org/10.1371/journal.pone.0170113>

Murakoshi, H., and R. Yasuda. 2012. Postsynaptic signaling during plasticity of dendritic spines. *Trends Neurosci.* 35:135–143. <https://doi.org/10.1016/j.tins.2011.12.002>

Ngo-Anh, T.J., B.L. Bloodgood, M. Lin, B.L. Sabatini, J. Maylie, and J.P. Adelman. 2005. SK channels and NMDA receptors form a  $\text{Ca}^{2+}$ -mediated feedback loop in dendritic spines. *Nat. Neurosci.* 8:642–649. <https://doi.org/10.1038/nn1449>

Nishiyama, J., and R. Yasuda. 2015. Biochemical computation for spine structural plasticity. *Neuron*. 87:63–75. <https://doi.org/10.1016/j.neuron.2015.05.043>

Nixon-Abell, J., C.J. Obara, A.V. Weigel, D. Li, W.R. Legant, C.S. Xu, H.A. Pasolli, K. Harvey, H.F. Hess, E. Betzig, et al. 2016. Increased spatio-temporal resolution reveals highly dynamic dense tubular matrices in the peripheral ER. *Science*. 354:aaf3928. <https://doi.org/10.1126/science.aaf3928>

Noguchi, J., M. Matsuzaki, G.C. Ellis-Davies, and H. Kasai. 2005. Spine-neck geometry determines NMDA receptor-dependent  $\text{Ca}^{2+}$  signaling in dendrites. *Neuron*. 46:609–622. <https://doi.org/10.1016/j.neuron.2005.03.015>

Oertner, T.G., and A. Matus. 2005. Calcium regulation of actin dynamics in dendritic spines. *Cell Calcium*. 37:477–482. <https://doi.org/10.1016/j.ceca.2005.01.016>

Ohadi, D., and P. Rangamani. 2019. Geometric control of frequency modulation of camp oscillations due to  $\text{Ca}^{2+}$ -bursts in dendritic spines. *bioRxiv*. doi:10.1101/520643 (Preprint posted January 15, 2019)

Ohadi, D., D.L. Schmitt, B. Calabrese, S. Halpain, J. Zhang, and P. Rangamani. 2019. Computational modeling reveals frequency modulation of calcium-camp/pka pathway in dendritic spines. *bioRxiv*. doi:10.1101521740 (Preprint posted January 16, 2019)

Ostroff, L.E., B. Botsford, S. Gindina, K.K. Cowansage, J.E. LeDoux, E. Klann, and C. Hoeffer. 2017. Accumulation of polyribosomes in dendritic spine heads, but not bases and necks, during memory consolidation depends on cap-dependent translation initiation. *J. Neurosci.* 37:1862–1872. <https://doi.org/10.1523/JNEUROSCI.3301-16.2017>

Ouyang, Y., M. Wong, F. Capani, N. Rensing, C.-S. Lee, Q. Liu, C. Neusch, M.E. Martone, J.Y. Wu, K. Yamada, et al. 2005. Transient decrease in F-actin may be necessary for translocation of proteins into dendritic spines. *Eur. J. Neurosci.* 22:2995–3005. <https://doi.org/10.1111/j.1460-9568.2005.04521.x>

Paulin, J.J., P. Haslehurst, A.D. Fellows, W. Liu, J.D. Jackson, Z. Joel, D.M. Cummings, and F.A. Edwards. 2016. Large and small dendritic spines serve different interacting functions in hippocampal synaptic plasticity and homeostasis. *Neural Plast.* 2016:6170509. <https://doi.org/10.1155/2016/6170509>

Rackham, O.J., K. Tsaneva-Atanasova, A. Ganesh, and J.R. Mellor. 2010. A  $\text{Ca}^{2+}$ -based computational model for NMDA receptor-dependent synaptic plasticity at individual post-synaptic spines in the hippocampus. *Front. Synaptic Neurosci.* 2:31.

Rangamani, P., M.G. Levy, S. Khan, and G. Oster. 2016. Paradoxical signaling regulates structural plasticity in dendritic spines. *Proc. Natl. Acad. Sci. USA*. 113:E5298–E5307. <https://doi.org/10.1073/pnas.1610391113>

Rochefort, N.L., and A. Konnerth. 2012. Dendritic spines: from structure to *in vivo* function. *EMBO Rep.* 13:699–708. <https://doi.org/10.1038/embor.2012.102>

Sabatini, B.L., and K. Svoboda. 2000. Analysis of calcium channels in single spines using optical fluctuation analysis. *Nature*. 408:589–593. <https://doi.org/10.1038/35046076>

Sabatini, B.L., M. Maravall, and K. Svoboda. 2001.  $\text{Ca}^{2+}$  signaling in dendritic spines. *Curr. Opin. Neurobiol.* 11:349–356. [https://doi.org/10.1016/S0959-4388\(00\)00218-X](https://doi.org/10.1016/S0959-4388(00)00218-X)

Sabatini, B.L., T.G. Oertner, and K. Svoboda. 2002. The life cycle of  $\text{Ca}^{2+}$  ions in dendritic spines. *Neuron*. 33:439–452. [https://doi.org/10.1016/S0896-6273\(02\)00573-1](https://doi.org/10.1016/S0896-6273(02)00573-1)

Santamaría, F., S. Wils, E. De Schutter, and G.J. Augustine. 2006. Anomalous diffusion in Purkinje cell dendrites caused by spines. *Neuron*. 52: 635–648. <https://doi.org/10.1016/j.neuron.2006.10.025>

Schmidt, H. 2012. Three functional facets of calbindin D-28k. *Front. Mol. Neurosci.* 5:25. <https://doi.org/10.3389/fnmol.2012.00025>

Schmidt, H., and J. Eilers. 2009. Spine neck geometry determines spino-dendritic cross-talk in the presence of mobile endogenous calcium binding proteins. *J. Comput. Neurosci.* 27:229–243. <https://doi.org/10.1007/s10827-009-0139-5>

Schmidt, H., S. Kunerth, C. Wilms, R. Strotmann, and J. Eilers. 2007. Spino-dendritic cross-talk in rodent Purkinje neurons mediated by endogenous  $\text{Ca}^{2+}$ -binding proteins. *J. Physiol.* 581:619–629. <https://doi.org/10.1113/jphysiol.2007.127860>

Segal, M. 2005. Dendritic spines and long-term plasticity. *Nat. Rev. Neurosci.* 6:277–284. <https://doi.org/10.1038/nrn1649>

Segal, M., and E. Korkotian. 2014. Endoplasmic reticulum calcium stores in dendritic spines. *Front. Neuroanat.* 8:64. <https://doi.org/10.3389/fnana.2014.00064>

Segal, M., A. Vlachos, and E. Korkotian. 2010. The spine apparatus, synaptotagmin, and dendritic spine plasticity. *Neuroscientist.* 16:125–131. <https://doi.org/10.1177/1073858409355829>

Sejnowski, T.J. 1977. Statistical constraints on synaptic plasticity. *J. Theor. Biol.* 69:385–389. [https://doi.org/10.1016/0022-5193\(77\)90146-1](https://doi.org/10.1016/0022-5193(77)90146-1)

Shouval, H.Z., M.F. Bear, and L.N. Cooper. 2002. A unified model of NMDA receptor-dependent bidirectional synaptic plasticity. *Proc. Natl. Acad. Sci. USA.* 99:10831–10836. <https://doi.org/10.1073/pnas.152343099>

Siesjö, B.K. 1990. Calcium in the brain under physiological and pathological conditions. *Eur. Neurol.* 30(Suppl 2):3–9, discussion:39–41. <https://doi.org/10.1159/000117184>

Song, S., K.D. Miller, and L.F. Abbott. 2000. Competitive Hebbian learning through spike-timing-dependent synaptic plasticity. *Nat. Neurosci.* 3: 919–926. <https://doi.org/10.1038/78829>

Spacek, J., and K.M. Harris. 1997. Three-dimensional organization of smooth endoplasmic reticulum in hippocampal CA1 dendrites and dendritic spines of the immature and mature rat. *J. Neurosci.* 17:190–203. <https://doi.org/10.1523/JNEUROSCI.17-01-00190.1997>

Standage, D., T. Trappenberg, and G. Blohm. 2014. Calcium-dependent calcium decay explains STDP in a dynamic model of hippocampal synapses. *PLoS One.* 9:e86248. <https://doi.org/10.1371/journal.pone.0086248>

Turrigiano, G. 2011. Too many cooks? Intrinsic and synaptic homeostatic mechanisms in cortical circuit refinement. *Annu. Rev. Neurosci.* 34: 89–103. <https://doi.org/10.1146/annurev-neuro-060909-153238>

Voorsluys, V., S.P. Dawson, Y. De Decker, and G. Dupont. 2019. Deterministic limit of intracellular calcium spikes. *Phys. Rev. Lett.* 122:088101. <https://doi.org/10.1103/PhysRevLett.122.088101>

Wacquier, B., L. Combettes, G.T. Van Nhieu, and G. Dupont. 2016. Interplay between intracellular  $Ca^{2+}$  oscillations and  $Ca^{2+}$ -stimulated mitochondrial metabolism. *Sci. Rep.* 6:19316. <https://doi.org/10.1038/srep19316>

Wilson, C.J., P.M. Groves, S.T. Kitai, and J.C. Linder. 1983. Three-dimensional structure of dendritic spines in the rat neostriatum. *J. Neurosci.* 3: 383–388. <https://doi.org/10.1523/JNEUROSCI.03-02-00383.1983>

Wu, Y., C. Whiteus, C.S. Xu, K.J. Hayworth, R.J. Weinberg, H.F. Hess, and P. De Camilli. 2017. Contacts between the endoplasmic reticulum and other membranes in neurons. *Proc. Natl. Acad. Sci. USA.* 114:E4859–E4867. <https://doi.org/10.1073/pnas.1701078114>

Wuytack, F., L. Raeymaekers, and L. Missiaen. 2002. Molecular physiology of the SERCA and SPCA pumps. *Cell Calcium.* 32:279–305. <https://doi.org/10.1016/S0143416002001847>

Yasuda, R. 2017. Biophysics of biochemical signaling in dendritic spines: Implications in synaptic plasticity. *Biophys. J.* 113:2152–2159. <https://doi.org/10.1016/j.biophys.2017.07.029>

Yasuda, H., A.L. Barth, D. Stellwagen, and R.C. Malenka. 2003. A developmental switch in the signaling cascades for LTP induction. *Nat. Neurosci.* 6:15–16. <https://doi.org/10.1038/nn985>

Yasuda, R., E.A. Nimchinsky, V. Scheuss, T.A. Pologruto, T.G. Oertner, B.L. Sabatini, and K. Svoboda. 2004. Imaging calcium concentration dynamics in small neuronal compartments. *Sci. STKE.* 2004:pl5.

Yeung, L.C., H.Z. Shouval, B.S. Blais, and L.N. Cooper. 2004. Synaptic homeostasis and input selectivity follow from a calcium-dependent plasticity model. *Proc. Natl. Acad. Sci. USA.* 101:14943–14948. <https://doi.org/10.1073/pnas.0405555101>

Yuste, R. 2010. *Dendritic Spines.* MIT Press, Cambridge, MA. <https://doi.org/10.7551/mitpress/9780262013505.001.0001>

Yuste, R., and W. Denk. 1995. Dendritic spines as basic functional units of neuronal integration. *Nature.* 375:682–684. <https://doi.org/10.1038/375682a0>

Yuste, R., A. Majewska, and K. Holthoff. 2000. From form to function: calcium compartmentalization in dendritic spines. *Nat. Neurosci.* 3: 653–659. <https://doi.org/10.1038/76609>

Zhou, Q., and M. Sheng. 2013. NMDA receptors in nervous system diseases. *Neuropharmacology.* 74:69–75. <https://doi.org/10.1016/j.neuropharm.2013.03.030>